PERGAMON

Journal of Structural Geology 24 (2002) 1937–1955

JOURNAL OF STRUCTURAL GEOLOGY

www.elsevier.com/locate/jstrugeo

The relation between grain size and $^{40}Ar/^{39}Ar$ date for Alpine white mica from the Siviez-Mischabel Nappe, Switzerland

Michelle J. Markley[a,*], Christian Teyssier[b], Mike Cosca[c]

[a]*Department of Earth and Environment, Mount Holyoke College, South Hadley, MA 01075, USA*
[b]*Department of Geology and Geophysics, University of Minnesota, Minneapolis, MI, USA*
[c]*Institut de Minéralogie et Géochimie, Université de Lausanne, Lausanne, Switzerland*

Received 15 March 2001; accepted 22 January 2002

Abstract

Variations in Alpine white mica $^{40}Ar/^{39}Ar$ dates from the cover units of the Siviez-Mischabel Nappe relate to regional variations in the thermal history of the nappe. We focus on three regions within the nappe: the central Siviez-Mischabel (CSM), the southern Siviez-Mischabel (SSM), and the eastern Siviez-Mischabel (ESM). Our approach weaves together observations of quartz and mica textures in thin section, the variation of $^{40}Ar/^{39}Ar$ date with grain size, considerations of the effective diffusion dimension (EDD) of argon in white mica, and a comparison of dates with diffusion model results. In the CSM, pressure solution of quartz and dislocation glide in mica accommodated Alpine deformation. Dates record mica growth during nappe emplacement from 40 to 36 Ma and do not vary with grain size. In the SSM and ESM, both mica and quartz show textures associated with dynamic recrystallization, and dates decrease with grain size. In the SSM, dates also agree with the timing of nappe emplacement, but in the ESM, dates significantly post-date the timing of nappe emplacement. A comparison of dates with diffusion model results supports inferences from rock fabrics that the SSM experienced higher peak temperatures than the CSM, even though dates from both units approximate the timing of mica growth. Dates obtained from the ESM, however, do not compare well with simple models, and the thermal evolution of this region of the nappe, in the neighborhood of the Simplon Fault Zone, is not well understood.

Keywords: Grain size; Alpine white mica; Siviez-Mischabel Nappe; quartz deformation mechanisms; 40Ar/39Ar dates; Effective diffusion dimension

1. Introduction

1.1. Project background and goals

Interpreting $^{40}Ar/^{39}Ar$ dates from deformed and metamorphosed terranes is difficult. Among samples from the same terrane, variations in thermal history, deformation history, lithology, and exposure to excess argon may account for variations in $^{40}Ar/^{39}Ar$ dates. In one such study, Markley et al. (1998) reported Oligocene and Eocene $^{40}Ar/^{39}Ar$ white mica dates obtained by step-heating of bulk separates from micaceous quartzites of the greenschist grade Siviez-Mischabel Nappe of the western Swiss Alps (Fig. 1). These dates vary with orogenic position. In the central and southern Siviez-Mischabel (CSM and SSM; Fig. 1), dates range from 40 to 36 Ma and agree well with independent estimates of the timing of ductile thrusting and emplacement of the Siviez-Mischabel Nappe in the Alpine orogenic welt. In the eastern Siviez-Mischabel (ESM; Fig. 1), however, dates range from 37 to 29 Ma, and some significantly post-date nappe emplacement.

Unusually good constraints exist for interpreting these regional differences in dates (Markley et al., 1998). White mica populations define the strong subhorizontal foliation and N–S transverse lineation associated with Eocene nappe emplacement, suggesting that mica grew synkinematically. Although identical geometric and metamorphic fabrics may form at different times in different positions in orogens, such a pronounced variation in the timing of nappe emplacement seems unlikely in this case. Therefore, the three regions (the CSM, SSM, and ESM) are assumed to share a common deformation history. The lithology of the samples is consistent and simple. Rock fabrics, white mica composition, and protolith considerations strongly suggest that the mica populations grew during a single deformation event and are free of argon isotopic inheritance. No evidence for contamination by excess argon exists.

Why then are white mica dates from the eastern reaches of the Siviez-Mischabel Nappe (the ESM) younger than the others? Markley et al. (1998) hypothesized that post-emplacement variations in the thermal history of different regions

* Corresponding author. Tel.: +1-413-438-2814; fax: +1-413-538-2239.
E-mail address: mmarkley@mtholyoke.edu (M.J. Markley).

0191-8141/02/$ - see front matter
PII: S0191-8141(02)00006-8

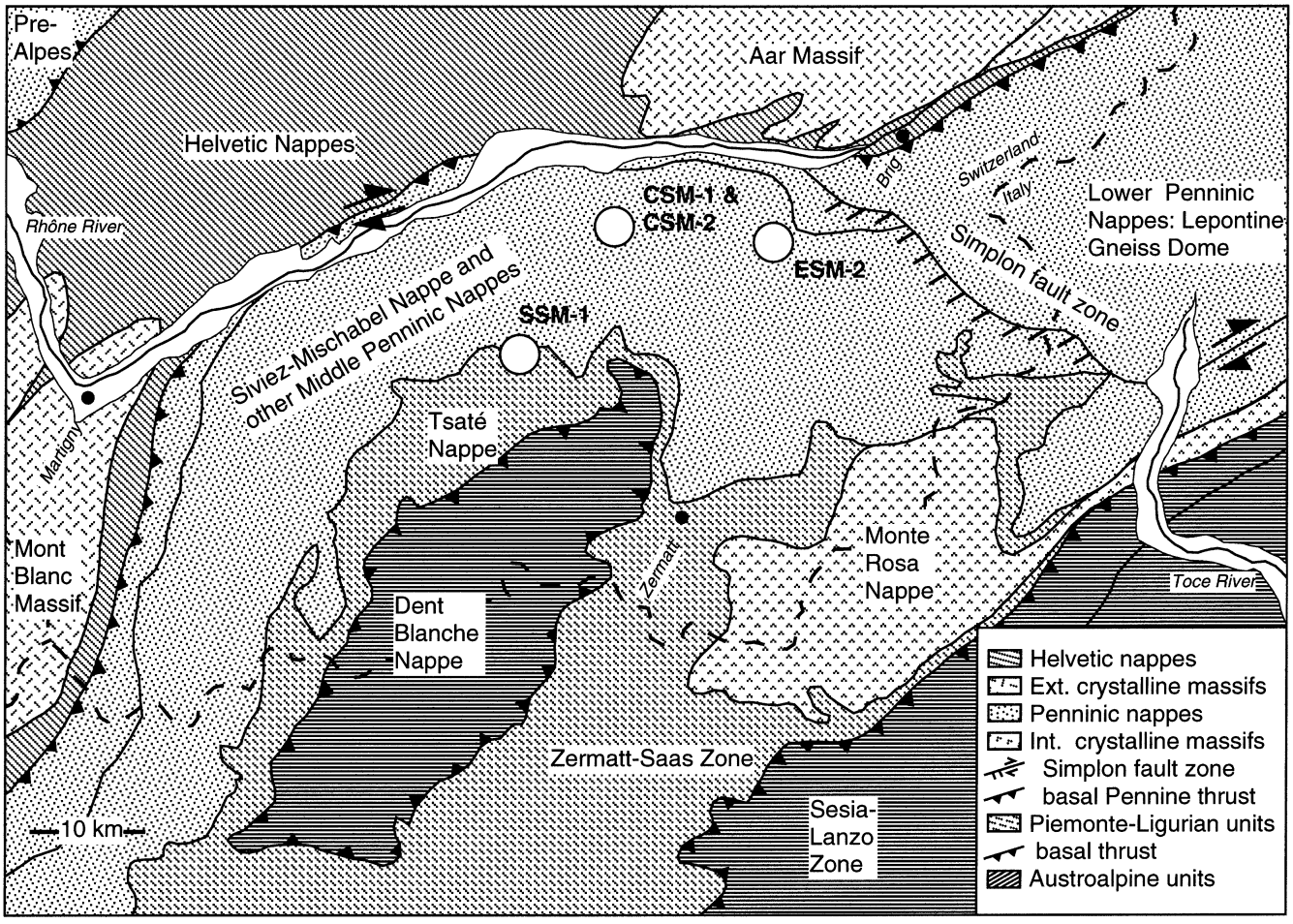

Fig. 1. Geologic map of the major tectonic units in the western Swiss and Italian Alps. Major Eocene thrust contacts shown are the basal Pennine thrust and the contact between Austroalpine units (Dent Blanche Nappe and Sesia–Lanzo Zone) and oceanic Piemonte–Ligurian units (Tsaté Nappe and Zermatt–Saas Zone). The Neogene Simplon Fault Zone accommodated both normal and transform motion.

of the nappe might account for the variations in $^{40}Ar/^{39}Ar$ white mica dates. Here we test that hypothesis using DIFFARG, a finite difference model that simulates the evolution of argon concentration and zoning in minerals (Wheeler, 1996). In particular, we explore the two following explanations for the observation that some samples show a variation of $^{40}Ar/^{39}Ar$ date with grain size, while other samples show no such variation: (1) regional variations in deformation mechanisms affected the effective diffusion dimension (EDD) of mica; or (2) the EDD of mica is the grain size itself, and regional thermal variations may have exerted a more direct control on dates. Although uncertainty over microstructural controls on the diffusion geometry of argon in white mica renders our tests non-unique, $^{40}Ar/^{39}Ar$ date variations appear to relate to the thermal history of the Siviez-Mischabel Nappe.

1.2. Literature review: the relation between $^{40}Ar/^{39}Ar$ and K–Ar white mica date and grain size

A number of experimental and field-oriented studies suggest that thermally activated volume diffusion of argon occurs in white micas, although it may not be the only important mechanism by which micas lose argon. Results of laser $^{40}Ar/^{39}Ar$ studies on argon isotopic zoning in micas (Phillips and Onstott, 1988; Scaillet et al., 1990; de Jong et al., 1992; Hodges et al., 1994) support two conclusions. First, in nature, volume diffusion of argon in white micas generally occurs parallel to the mica basal {001} cleavage plane and is best described by a cylindrical diffusion geometry (Gilletti, 1974). The effective diffusion dimension (EDD) of white mica therefore relates to its diameter parallel to the basal plane (Gilletti, 1974; Hames and Bowring, 1994). Second, the EDD of argon in muscovite can be at least 500 μm (Hodges et al., 1994). Evidence that the EDD of argon in many minerals is much smaller than the grain size, however, permeates the literature on argon dates. For example, Wright et al. (1991) showed that the effective diffusion dimension of biotite may be smaller than large grains (biotite EDD ≈ 450 μm). Also, studies on feldspars support models of geometrically complex diffusion domains unrelated to grain size (Lovera et al., 1989). Lee (1995) noted that crystal defects such as dislocations, exsolution lamellae, micropores, microfractures, and fission tracks in

mineral grains may provide fast diffusion pathways that compete with volume diffusion. He suggested that indirect evidence for multipath diffusion may be: (1) isotopic zoning in grains that does not correspond to that expected for volume diffusion, or (2) a lack of correlation between date and grain size. Recent $^{40}Ar/^{39}Ar$ evidence supports such microstructurally controlled diffusion pathways (Kramar et al., 2001; Mulch et al., 2001).

The relation between $^{40}Ar/^{39}Ar$ date and grain size may therefore constrain interpretations of dates. Although laser technology is changing the use of traditional techniques in $^{40}Ar/^{39}Ar$ mineral dating (for example, Reddy et al., 1996; Kramar et al., 2001), most tectonic studies report data from bulk mineral separates obtained from crushed and sieved rocks. White mica dates are commonly obtained on groups of grains that are hand-picked from a sieved size fraction. Here we review the results of some studies, like ours, that report $^{40}Ar/^{39}Ar$ mica data for separates from a range of size fractions.

Single generations of white mica in slowly cooled terranes offer the simplest example of a clear and meaningful relation between $^{40}Ar/^{39}Ar$ white mica date and grain size. In such retrograde systems, mineral closure temperature (T_c) depends strongly on the EDD of the mineral (Dodson, 1973). Hess et al. (1993) documented this phenomenon in a careful study of the relation between $^{40}Ar/^{39}Ar$ white mica date and grain size in a young granite in the Caucasus Mountains. They showed that dates decrease with grain size over a range of a few million years in a manner consistent with volume diffusion theory and with independent constraints on the thermal history of the granite. Hess et al. (1993) interpreted the range of dates to reflect the progressive closure of increasingly smaller grains to argon diffusion during cooling of the granite. These dates are therefore cooling ages because they record the cooling of the rocks, rather than the growth of the grains.

For low grade (anchizone) metamorphic settings, published data on the relation between $^{40}Ar/^{39}Ar$ dates and grain size show a broad array of results. In these settings, detrital and neocrystallized sheet silicates commonly coexist. Understanding dates from these diverse populations of mica, which are often quite small, has been a matter of debate and innovation for two decades (Frank and Stettler, 1979; Hunziker, 1986; Reuter and Dallmeyer, 1987; Foland et al., 1992; Dong et al., 1997; Jaboyedoff and Cosca, 1999), and a review of this literature is outside the realm of this study. For white mica grown during prograde greenschist and higher grade metamorphism, published data on the relation between mica date and grain size are also equivocal. Hammerschmidt and Stöckert (1987) reported K–Ar and $^{40}Ar/^{39}Ar$ white mica dates, from Hercynian schists in the southern Alps, that decrease as a function of grain size. They argued that this relation reflects post-metamorphic cooling, similar to the Caucasus granite example discussed above. Kelley (1988) reported K–Ar dates from the Moine thrust zone that also decrease as a function of grain size. Although this data set is complicated, he attributed the relation between date and grain size to a combination of synkinematic recrystallization and thermally activated volume diffusion. In contrast, Itaya and Takasugi (1988) reported K–Ar white mica dates from the Sanbagawa schists of Japan that increase with decreasing grain size. They interpreted this unusual relation as reflecting more intense recrystallization of larger micas, although the authors unfortunately do not support this interpretation with any compositional or microstructural data. In all three studies, the range of dates between different grain sizes is in the order of 10 million years.

In many polymetamorphic rocks, petrographic observations and chemical analyses reveal two distinct mica generations that grew under different metamorphic and kinematic conditions. Ironically, these complicated metamorphic settings appear to yield an extremely consistent relation between mica date and grain size because the younger generation of micas is commonly much smaller than the older generation. Dating different mica size fractions separated from polymetamorphic rocks is an approach that has been taken by Zingg and Hunziker (1990) in the Insubric Line of the central Alps, Dunlap et al. (1991) in the Arltunga Nappe complex of central Australia, Cosca et al. (1992) in the pre-Alpes, and West and Lux (1993) in the Norumbega Fault zone of the northern Appalachians. These studies collectively show a common pattern of decreasing $^{40}Ar/^{39}Ar$ mica date with decreasing grain size. The range of dates, however, commonly spans tens to hundreds of million of years and reflects, at least in part, the time gap between two distinct and commonly unrelated tectonic events. Because it is difficult to completely separate the two generations of mica, the dates from the smallest grain size fraction are generally interpreted as yielding a maximum age for the younger event, and the dates from the largest grain size fraction are interpreted as yielding a minimum age for the older event. This interpretation, however, does not constrain the possible effects of thermally activated argon loss from the youngest, smaller generation of mica.

Studies on more complicated settings than those discussed above also yield the same relation. Lo and Onstott (1995) showed that in the Taiwan Mountain Belt, polymetamorphic samples show a decrease of muscovite and biotite date with size fraction, even when possible recrystallization and generational mixing effects are isolated. Goodwin and Renne (1991) showed that grain size reduction during mylonitization and synchronous thermal resetting of mica is also associated with a decrease of biotite date with size fraction. Therefore, the positive correlation between date and grain size appears also to be characteristic of argon loss by volume diffusion during thermal resetting of mica. With the advent of $^{40}Ar/^{39}Ar$ ultraviolet laser dating technology, new studies may place more emphasis on the relation between date, grain size, composition, and microstructural setting (for example, Mulch et al., 2001). In our study, however, samples are too young (and concentrations of

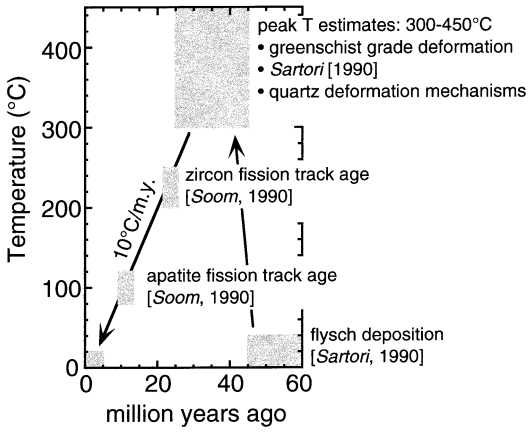

Fig. 2. Proposed thermal history of the Siviez-Mischabel Nappe.

radiogenic argon too low) to be suitable for current laser dating techniques.

2. The Siviez-Mischabel Nappe

2.1. Thermal and geologic history

The Alpine thermal history of the Siviez-Mischabel Nappe (Argand, 1916; Escher, 1988) is constrained by both isotopic and field data (Fig. 2). On the basis of lithologic correlation with other units in the western Alps, Sartori (1990) argued that black flysch units of the Série du Barrhorn in the Siviez-Mischabel cover sequence are middle to late Eocene in age. Following Eocene sedimentation, the Siviez-Mischabel underwent rapid burial and greenschist facies metamorphism during the Alpine collisional event.

Rock fabrics from the Siviez-Mischabel cover units suggest that white mica growth occurred during peak

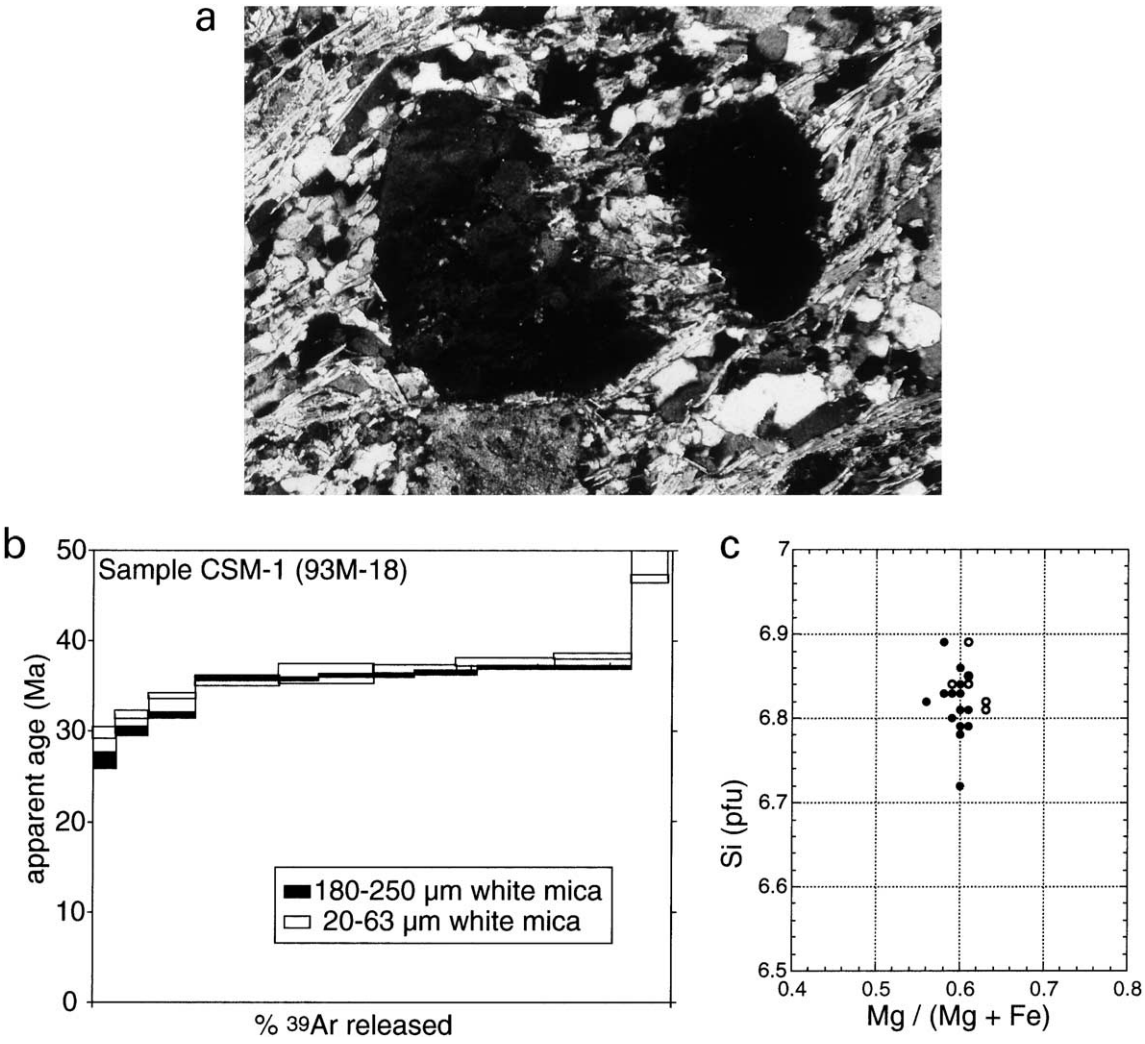

Fig. 3. Sample CSM-1 of the central Siviez-Mischabel Nappe. (a) Photomicrograph, width of view is approximately 1.3 mm. White mica defines Alpine foliation, and a detrital quartz grain is fractured in half. (b) $^{40}Ar/^{39}Ar$ white mica dates obtained from the 20–63 and 180–250 μm fractions. Date does not vary as a function of grain size. (c) Microprobe analyses on mica grains in thin section show that compositions of the two different grain sizes are indistinguishable.

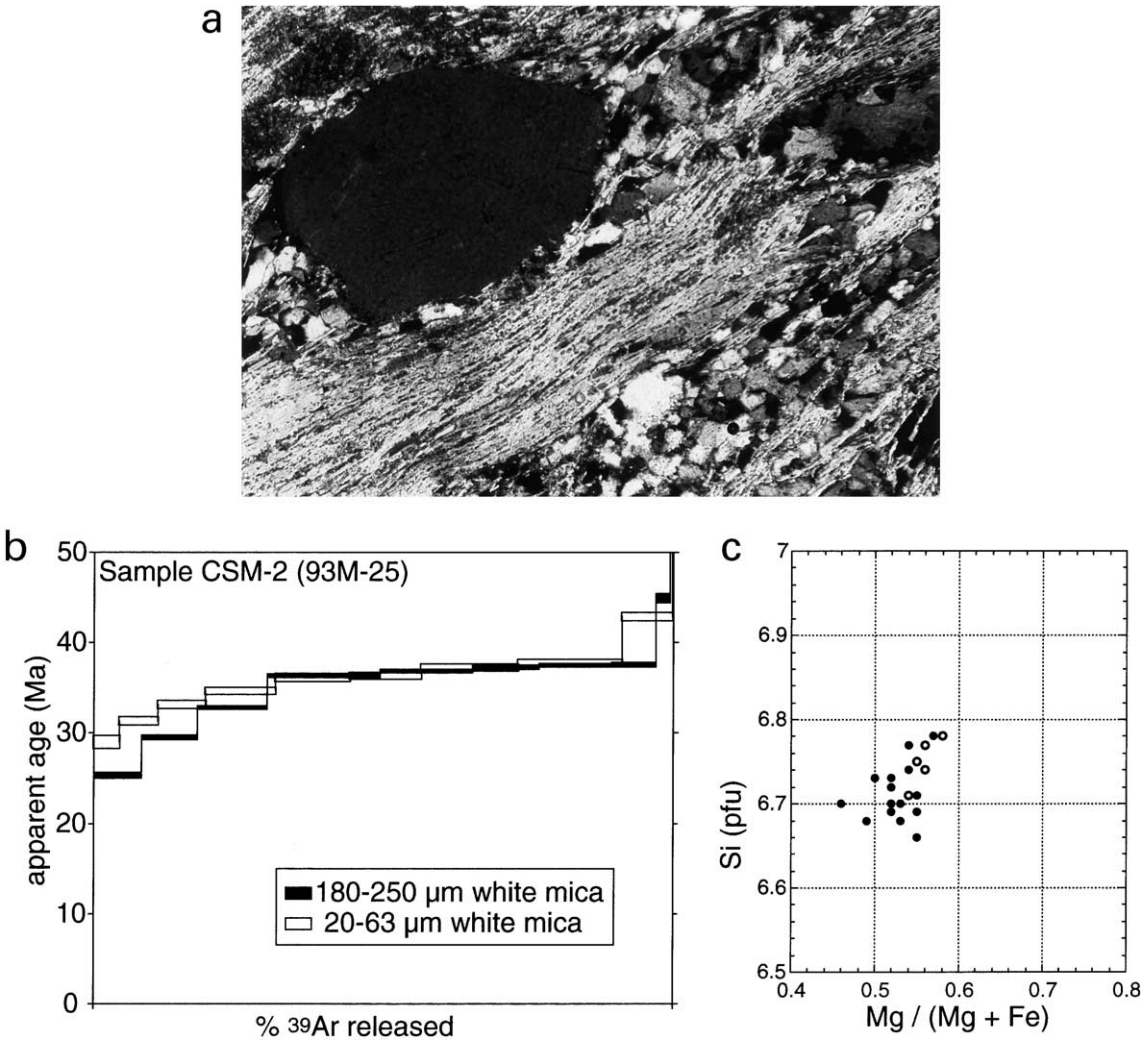

Fig. 4. Sample CSM-2 of the central Siviez-Mischabel Nappe. (a) Photomicrograph, width of view is approximately 1.3 mm. White mica defines Alpine foliation, and a detrital quartz grain remains. (b) $^{40}Ar/^{39}Ar$ white mica dates obtained from the 20–63 and 180–250 μm fractions. Date does not vary with grain size. (c) Microprobe analyses on mica grains in thin section show that compositions of the two different grain sizes are indistinguishable.

metamorphism and deformation (Markley et al., 1998). A few Rb–Sr dates of approximately 40 Ma from synkinematic white micas in another region of the nappe constrain the timing of this mica growth (Barnicoat et al., 1995). The oldest $^{40}Ar/^{39}Ar$ white mica dates from cover units the Siviez-Mischabel Nappe agree well with this estimate for the timing of peak metamorphic conditions (Markley et al., 1998). Sartori (1990) estimated peak temperatures at 350–450 °C, although he based this estimate on an unconventional barometer (Mg substitution in the chloritoid–chlorite pair). Deformation mechanisms of quartz in the Siviez-Mischabel provide a lower and similarly unconventional estimate of peak metamorphic temperatures. The transition from pressure solution to dislocation creep and recovery mechanisms, as observed between the different regions of the Siviez-Mischabel Nappe (Markley et al., 1998), occurs at approximately 300 °C for natural strain rates (Wilson, 1973; Kerrich et al., 1977).

The retrograde thermal history of the Siviez-Mischabel is comparatively well constrained by the zircon and apatite fission track data of Soom (1990). Together, the data summarized in Fig. 2 suggest that the Siviez-Mischabel Nappe cooled from peak metamorphic conditions to its present surface exposure at a rate of 10 °C/m.y. This figure omits two potentially significant tectonic events that may have thermally disturbed the eastern reaches of the Siviez-Mischabel nappe. Some magmatism occurred in the lower Penninic Nappes (Fig. 1) at 30 Ma (Steck and Hunziker, 1994; Schärer et al., 1996), and extension accrued along the low-angle Simplon fault zone (Fig. 1) at approximately 15 Ma (Graseman and Mancktelow, 1993; Steck and Hunziker, 1994).

2.2. Sample descriptions and dates

Below, we summarize petrographic, $^{40}Ar/^{39}Ar$ isotopic, and compositional observations on white mica in four samples from the Permo–Triassic metapelites and

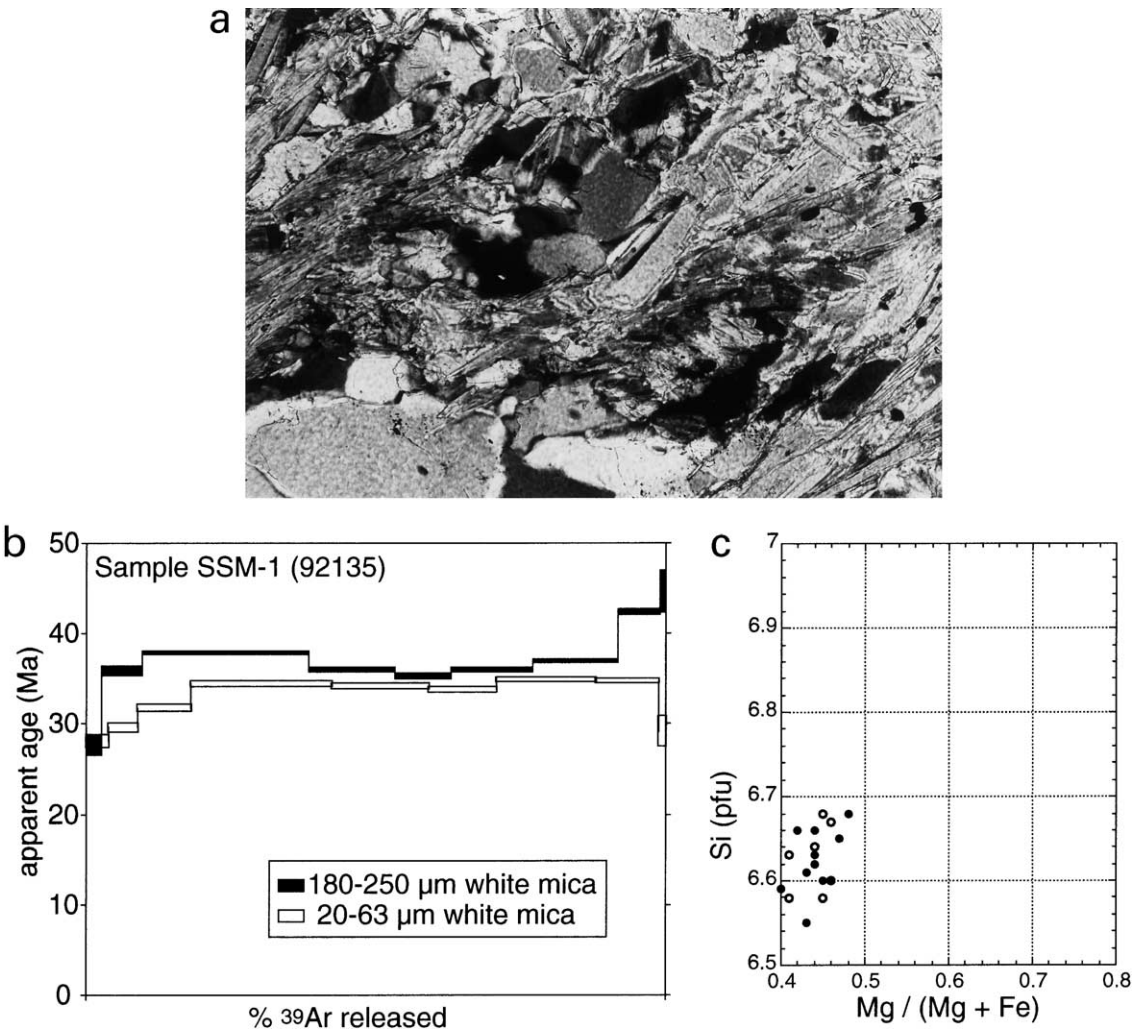

Fig. 5. Sample SSM-1 of the southern Siviez-Mischabel Nappe. (a) Photomicrograph, width of view is approximately 1.3 mm. White mica defines Alpine foliation, and quartz is recrystallized. (b) $^{40}Ar/^{39}Ar$ white mica dates obtained from the 20–63 and 180–250 μm fractions. Date decreases as a function of grain size. (c) Microprobe analyses on mica grains in thin section show that compositions of the two different grain sizes are indistinguishable.

metasandstones of the Siviez-Mischabel Nappe: samples CSM-1 (Fig. 3) and CSM-2 (Fig. 4) from the central Siviez-Mischabel Nappe (Fig. 1); sample SSM-1 (Fig. 5) from the southern Siviez-Mischabel Nappe (Fig. 1); and sample ESM-2 (Fig. 6) from the eastern Siviez-Mischabel Nappe (Fig. 1). Table 1 contains raw microprobe data plotted in Figs. 3c, 4c, 5c and 6c. Table 2 contains the raw $^{40}Ar/^{39}Ar$ data, which are also plotted in Figs. 3b, 4b, 5b and 6b. These data are corrected for blanks, mass discrimination, radioactive decay, and interfering isotopic reactions. Markley et al. (1998) report separation, irradiation, and $^{40}Ar/^{39}Ar$ step-heating procedures for mica separates. Although we base our discussion of these data on total gas ages (Table 2), we present the release spectra in Figs. 3–6 so that the reader can further evaluate the data. A 2σ error of 0.2–0.6 m.y. is associated with total gas ages.

Sample CSM-1. This sample (Fig. 3a) contains white mica (30%), quartz (65%), and detrital potassium feldspar (5%). White mica occurs in two settings: (1) in large aggregate bands that define foliation, and (2) as individual grains within the quartz layers. In the first setting, mica grains 50–400 μm in length have relatively small aspect ratios (3:1) and a grainy texture. Smaller grains are oriented at large angles to foliation. In the second setting, mica grains occur as 20–200-μm-long thin plates (aspect ratios of approximately 10:1) oriented parallel to the foliation defined by aggregate bands. Large detrital quartz grains are commonly preserved and show pitted edges and pressure shadows of smaller recrystallized quartz grains and mica beards. Smaller 100 μm size quartz grains are slightly elongate parallel to foliation. These smaller quartz grains show well-developed triple grain junctions, straight edges, and uniform extinction.

The $^{40}Ar/^{39}Ar$ date of the smaller mica size fraction (20–63 μm) is 40 Ma, and the date of the larger size fraction (180–250 μm) is 39 Ma (Table 2). These two dates are statistically indistinguishable. Juxtaposition of the two release spectra (Fig. 3b) further emphasizes the similarity

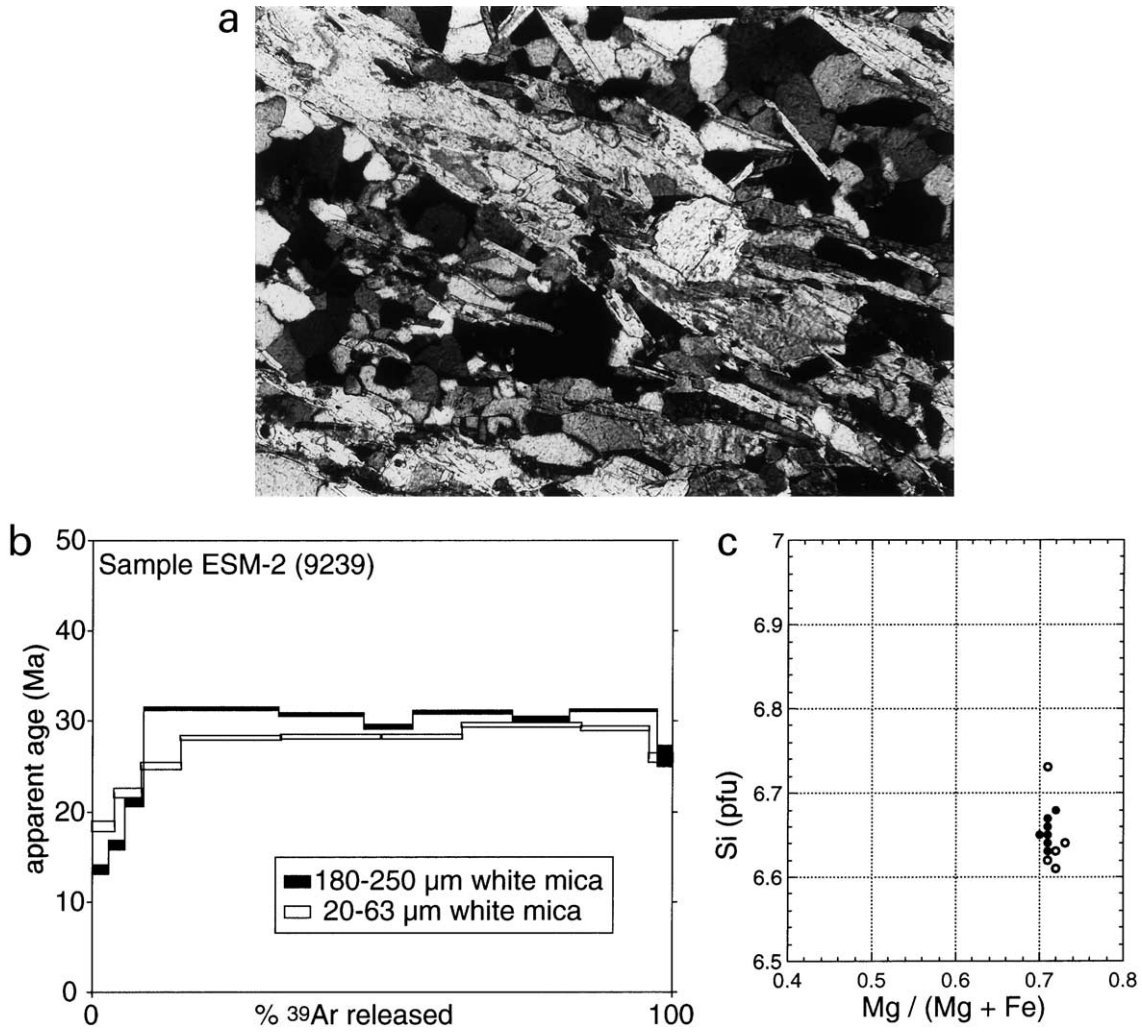

Fig. 6. Sample ESM-2 of the Eastern Siviez-Mischabel Nappe. (a) Photomicrograph, width of view is approximately 1.3 mm. White mica defines Alpine foliation, and quartz is recrystallized. (b) $^{40}Ar/^{39}Ar$ white mica dates obtained from the 20–63 and 180–250 μm fractions. Date decreases with grain size. (c) Microprobe analyses on mica grains in thin section show that compositions of the two different grain sizes are indistinguishable.

of the two dates. Microprobe analyses of white mica in thin sections in both settings (Fig. 3c) shows that mica composition is phengitic and does not vary with setting or grain size.

Sample CSM-2. This sample (Fig. 4a) contains white mica (30%), quartz (65%), detrital potassium feldspar (5%), and minor calcite/ankerite and detrital zircon. Textures of both mica and quartz are identical to those described above for sample CSM-1. The $^{40}Ar/^{39}Ar$ date of the smaller mica size fraction is 37 Ma, the larger size fraction 36 Ma (Table 2). Again, these two dates are statistically indistinguishable (Fig. 4b), and microprobe analyses show that the two size fractions are also compositionally alike (Fig. 4c).

Sample SSM-1. This sample (Fig. 5a) contains white mica (80%), quartz (20%), and minor opaque minerals and detrital zircon. Complex aggregates of mica grains define foliation. Most mica grains in these aggregates range in length between 200 and 500 μm and are clear, rather than grainy. Some smaller mica grains within these aggregates lie at large angles to foliation. Approximately equant quartz grains (100–200 μm in diameter) occur in layers between mica aggregates. These quartz grains show a polygonal fabric defined by triple-grain junctions, straight grain boundaries, and relatively uniform extinction. The $^{40}Ar/^{39}Ar$ date of the smaller mica size fraction is 34 Ma, the larger size fraction 37 Ma (Table 2). These two dates are statistically distinct (Fig. 5b), although microprobe analyses show that the two size fractions are compositionally alike (Fig. 5c).

Sample ESM-2. This sample (Fig. 6a) contains white mica (40%), quartz (60%), and minor potassium feldspar. Large Alpine white mica grains are clear and range in length from 100 to 500 μm and have aspect ratios ranging from 1:1 to 1:10. These mica grains define foliation but show a range of orientations. Mica grains with the smallest aspect ratios account for most of the mica grains at large angles to foliation. Smaller mica grains occur in the quartz matrix, which is composed of <50–100-μm-wide quartz grains. Quartz

Table 1
Raw microprobe data from thin sections

SiO_2	TiO_2	Al_2O_3	Cr_2O_3	FeO	MnO	MgO	BaO	CaO	Na_2O	K_2O	Total
Sample CSM-1 white mica, <60 μm grain diameters											
50.9	0.07	26.5	0.00	5.0	0.02	3.2	0.00	0.01	0.00	10.2	95.9
58.2	0.08	20.4	0.00	4.4	0.00	2.6	0.00	0.00	0.03	9.6	95.3
49.9	0.03	24.5	0.02	5.1	0.00	3.0	0.06	0.00	0.04	11.4	94.0
50.9	0.00	26.5	0.01	4.9	0.03	3.2	0.00	0.00	0.00	10.4	95.9
50.6	0.09	25.7	0.00	5.7	0.00	3.1	0.00	0.00	0.02	10.5	95.6
51.3	0.04	26.7	0.00	5.1	0.04	3.1	0.00	0.04	0.01	9.6	96.0
50.7	0.03	26.1	0.05	5.2	0.03	3.0	0.00	0.00	0.00	10.1	95.2
49.7	0.05	25.0	0.03	5.8	0.03	3.0	0.02	0.03	0.02	11.1	94.8
Sample CSM-1 white mica, >200 μm grain diameters											
49.5	0.00	25.6	0.02	5.3	0.01	3.0	0.26	0.03	0.03	11.2	94.9
49.3	0.08	25.5	0.00	5.1	0.00	3.0	0.00	0.06	0.03	10.9	94.1
48.8	0.00	26.1	0.02	5.3	0.02	2.9	0.08	0.01	0.00	11.2	94.6
49.6	0.02	25.0	0.00	5.4	0.00	3.1	0.00	0.00	0.04	11.3	94.4
49.5	0.02	25.2	0.02	5.3	0.02	3.0	0.00	0.00	0.04	11.4	94.5
48.8	0.13	24.3	0.00	6.4	0.00	3.0	0.01	0.03	0.01	10.8	93.5
48.8	0.09	24.3	0.00	5.3	0.00	3.0	0.00	0.03	0.03	10.8	92.3
49.9	0.00	25.0	0.00	5.2	0.03	3.0	0.04	0.01	0.06	11.4	94.7
49.4	0.01	25.1	0.03	5.4	0.05	2.9	0.00	0.08	0.03	10.8	93.8
50.1	0.02	24.3	0.01	6.0	0.00	3.1	0.00	0.02	0.00	11.1	94.7
49.8	0.00	25.1	0.01	5.4	0.04	3.1	0.11	0.01	0.04	11.1	94.7
49.9	0.14	25.5	0.03	5.3	0.02	3.0	0.00	0.00	0.03	11.3	95.2
49.7	0.03	25.7	0.00	5.3	0.02	2.9	0.00	0.02	0.03	11.1	94.8
49.1	0.06	25.9	0.00	5.0	0.04	2.8	0.00	0.09	0.03	10.5	93.5
49.7	0.12	24.9	0.01	5.8	0.04	3.1	0.00	0.08	0.01	11.0	94.7
50.0	0.15	25.7	0.03	5.1	0.02	3.0	0.05	0.00	0.03	11.2	95.2
Sample CSM-2 white mica, <60 μm grain diameters											
49.8	0.09	26.7	0.00	5.9	0.00	2.8	0.00	0.02	0.03	9.8	95.1
49.5	0.02	27.1	0.00	6.0	0.00	2.7	0.00	0.05	0.00	9.8	95.1
48.1	0.13	25.2	0.00	6.0	0.03	2.9	0.00	0.00	0.04	10.5	92.8
49.7	0.00	26.6	0.00	6.2	0.01	2.8	0.00	0.03	0.00	9.9	95.3
49.9	0.00	26.1	0.03	6.3	0.01	3.0	0.00	0.10	0.02	9.8	95.2
50.2	0.01	26.6	0.00	5.8	0.01	3.0	0.00	0.00	0.01	9.8	95.4
Sample CSM-2 white mica, >200 μm grain diameters											
49.5	0.03	25.9	0.00	5.8	0.00	2.5	0.00	0.03	0.03	11.4	95.2
50.7	0.04	27.2	0.00	6.8	0.02	2.6	0.04	0.02	0.02	10.5	97.9
49.8	0.00	26.7	0.02	6.7	0.01	2.7	0.00	0.01	0.03	10.0	96.0
49.1	0.04	26.2	0.02	7.9	0.00	2.5	0.00	0.07	0.01	10.0	95.8
49.1	0.07	27.1	0.00	6.2	0.00	2.8	0.00	0.02	0.02	10.4	95.7
49.3	0.03	27.0	0.00	5.9	0.01	2.7	0.00	0.00	0.00	10.6	95.5
49.0	0.08	26.7	0.01	6.4	0.00	2.6	0.00	0.02	0.02	9.9	94.7
49.2	0.00	26.4	0.00	6.7	0.01	2.7	0.00	0.03	0.01	10.1	95.2
49.2	0.04	26.6	0.02	6.5	0.03	2.7	0.00	0.03	0.01	10.3	95.5
49.0	0.00	26.3	0.00	6.4	0.01	2.7	0.00	0.01	0.02	10.1	94.6
49.2	0.00	26.8	0.02	6.4	0.01	2.5	0.09	0.01	0.00	10.4	95.5
48.9	0.00	25.9	0.00	6.2	0.00	2.7	0.00	0.02	0.03	10.7	94.5
49.1	0.16	26.4	0.01	7.1	0.00	2.6	0.08	0.00	0.01	10.4	95.8
49.4	0.03	26.9	0.00	6.0	0.00	2.7	0.00	0.01	0.00	10.3	95.5
49.3	0.06	27.2	0.03	6.2	0.01	2.6	0.00	0.01	0.03	10.0	95.4
50.0	0.04	26.1	0.00	6.1	0.01	3.0	0.00	0.00	0.01	10.1	95.3
Sample ESM-2 white mica, <60 μm grain diameters											
50.9	0.00	28.9	0.00	2.8	0.05	2.5	0.05	0.03	0.05	11.5	96.8
50.1	0.00	29.8	0.02	3.0	0.00	2.8	0.05	0.02	0.08	11.3	97.0
50.1	0.00	29.3	0.02	2.7	0.03	2.8	0.00	0.00	0.05	11.6	96.6
49.0	0.00	29.1	0.02	2.8	0.00	2.6	0.00	0.00	0.04	11.4	95.0
50.1	0.00	29.5	0.04	2.8	0.00	2.7	0.00	0.00	0.03	11.5	96.6
50.1	0.00	29.8	0.00	2.9	0.00	2.6	0.00	0.01	0.05	11.4	96.9
Sample ESM-2 white mica, >200 μm grain diameters											
50.5	0.00	29.4	0.00	2.8	0.01	2.6	0.00	0.04	0.02	11.1	96.5
50.2	0.05	29.4	0.02	2.9	0.00	2.6	0.00	0.02	0.03	11.3	96.6
50.3	0.00	29.6	0.01	2.9	0.00	2.6	0.00	0.04	0.01	11.0	96.5
50.4	0.08	29.4	0.03	2.9	0.02	2.6	0.02	0.04	0.07	11.2	96.8

Table 1 (*continued*)

SiO_2	TiO_2	Al_2O_3	Cr_2O_3	FeO	MnO	MgO	BaO	CaO	Na_2O	K_2O	Total
50.3	0.00	29.1	0.04	3.0	0.01	2.7	0.05	0.04	0.04	11.3	96.6
50.2	0.07	29.4	0.02	2.9	0.01	2.6	0.09	0.06	0.04	11.2	96.6
53.6	0.08	27.1	0.00	2.8	0.01	2.4	0.00	0.02	0.05	10.4	96.4
50.3	0.00	29.5	0.01	2.8	0.00	2.6	0.27	0.05	0.03	11.0	96.5
50.3	0.00	29.5	0.00	2.8	0.00	2.6	0.00	0.01	0.05	11.3	96.6
50.4	0.06	29.3	0.03	2.9	0.02	2.7	0.00	0.01	0.02	11.5	96.9
50.2	0.02	29.5	0.00	2.9	0.01	2.7	0.05	0.03	0.09	11.4	96.9
50.5	0.07	29.4	0.01	2.8	0.01	2.6	0.08	0.05	0.04	11.1	96.8
49.9	0.02	29.4	0.00	2.9	0.04	2.6	0.00	0.02	0.04	11.1	96.1
Sample SSM-1 white mica, <60 μm grain diameters											
48.6	0.00	28.1	0.02	6.6	0.02	2.1	0.00	0.07	0.05	10.0	95.6
49.0	0.00	27.4	0.02	6.7	0.00	2.2	0.05	0.02	0.05	10.2	95.5
48.2	0.00	27.1	0.01	7.1	0.01	2.1	0.07	0.00	0.05	10.0	94.6
48.7	0.10	28.2	0.04	6.8	0.03	2.1	0.00	0.03	0.07	10.3	96.4
48.2	0.00	27.7	0.03	7.6	0.00	1.9	0.06	0.04	0.04	10.3	95.8
47.7	0.08	26.5	0.00	7.7	0.03	2.1	0.00	0.00	0.04	9.8	94.1
47.0	0.00	25.8	0.01	6.7	0.00	2.1	0.00	0.04	0.06	9.9	91.7
Sample SSM-1 white mica, >200 μm grain diameters											
48.3	0.00	27.5	0.02	7.9	0.00	2.0	0.14	0.01	0.02	10.0	95.9
48.2	0.00	26.6	0.04	7.2	0.00	2.0	0.10	0.00	0.01	10.4	94.5
47.8	0.03	26.8	0.00	7.0	0.00	2.1	0.00	0.00	0.06	10.3	94.1
48.6	0.00	27.9	0.03	6.6	0.01	2.0	0.06	0.00	0.05	10.1	95.3
50.9	0.03	29.1	0.01	6.5	0.00	2.2	0.00	0.02	0.08	9.8	98.6
48.5	0.04	26.6	0.00	6.7	0.00	2.3	0.00	0.00	0.04	10.2	94.4
48.7	0.03	27.8	0.02	6.8	0.01	2.0	0.00	0.00	0.05	10.6	95.9
48.3	0.02	27.2	0.02	7.4	0.01	2.1	0.00	0.06	0.03	10.2	95.4
47.3	0.01	27.4	0.00	7.5	0.00	2.1	0.00	0.08	0.05	10.0	94.4
49.4	0.00	27.4	0.00	7.4	0.02	2.1	0.00	0.07	0.02	10.3	96.8
46.9	0.05	26.7	0.00	6.6	0.01	2.0	0.04	0.04	0.04	10.4	92.9
7.1	0.00	26.9	0.01	6.4	0.01	2.1	0.07	0.08	0.06	10.4	93.1

grains are polygonal and display uniform extinction. Their boundaries are straight and meet at triple-grain junctions. Potassium feldspar grains are rare and show the same size and texture as the quartz grains, with which they occur. The $^{40}Ar/^{39}Ar$ date of the smaller mica size fraction is 28 Ma, the larger size fraction 30 Ma (Table 2). These two dates are statistically distinct (Fig. 6b), although microprobe analyses show that the two size fractions are compositionally alike (Fig. 6c).

2.3. Discussion: significance of sample fabrics

Quartz textural variations among the four samples suggest that samples from the eastern and southern Siviez-Mischabel experienced higher peak temperatures than samples from the central Siviez-Mischabel. Samples ESM-2 and SSM-1 show polygonal quartz fabric. Quartz crystals in these samples are of uniform grain size, and grain boundaries meet in triple junctions. Quartz grain boundaries may be wavy or straight, extinction may be undulose or uniform, and grains may be equant or slightly elongated. These quartz microstructures reflect variable relative contributions of dislocation glide and recovery processes during crystal plastic deformation (Knipe, 1989). Samples CSM-1 and CSM-2, however, preserve detrital quartz grains. Pitted quartz grain boundaries and neighboring pressure shadows containing smaller quartz crystals are typically associated with the dissolution and reprecipitation of quartz during pressure solution (McClay, 1977). Experimental studies on quartz deformation show that the transition between deformation mechanisms, such as pressure solution and crystal plasticity, occurs in response to variations in temperature, strain rate, stress, water content, and grain size (Knipe, 1989). The interpretation of variations in quartz microstructure in the GSBN as reflecting lower temperatures in the central Siviez-Mischabel than in the eastern and southern Siviez-Mischabel is consistent with experimental results.

The significance of mica textures is more difficult to interpret because of the dearth of experimental work on deformed mica. Experiments on mica suggest that it deforms mainly by kinking, fracturing, and dislocation glide along its basal plane (Wilson and Bell, 1979; Bell and Wilson, 1981; Christofferson and Kronenberg, 1993; Shea and Kronenberg, 1993). But mica recrystallization or continuous dissolution and neocrystallization are mechanisms favored by workers who have focused on samples deformed naturally during sub-greenschist and higher grades of metamorphism (Etheridge and Hobbs, 1974; Vernon, 1977; Bell, 1978; Behrmann, 1984; Dunlap,

Table 2
Raw $^{40}Ar/^{39}Ar$ data. Steps with $\%^{40}Ar^* < 10$ are excluded (* = radiogenic)

Temp (°C)	$^{40}Ar^*/^{39}Ar$	$^{36}Ar/^{39}Ar$	$^{37}Ar/^{39}Ar$	^{40}Ar (mol ($\times 10^{-14}$))	$\%^{40}Ar^*/\%^{39}Ar$	Rel. age ± 2 σ (Ma)	
SSM-1 20–63 μm; $J = 0.002552 \pm 0.000006$; weight = 2.56 mg							
800	6.16	0.01418	0.6929	23.7	59.8	3.8	28.1 ± 0.6
850	6.48	0.00953	0.4165	28.2	70.0	5.1	29.6 ± 0.4
900	6.96	0.00780	0.1998	51.4	75.3	9.3	31.8 ± 0.4
950	7.56	0.00398	0.0937	126.6	86.6	24.2	34.5 ± 0.2
975	7.50	0.00448	0.1131	88.6	85.1	16.7	34.2 ± 0.4
1000	7.41	0.00416	0.1854	60.5	85.9	11.7	33.8 ± 0.4
1050	7.66	0.00262	0.1056	86.3	90.9	17.1	34.9 ± 0.2
1100	7.62	0.00305	0.1531	55.8	89.5	10.9	34.8 ± 0.2
1350	6.39	0.02055	0.7960	9.6	51.8	1.3	29.2 ± 1.6
Total gas age = 33.7 ± 0.4 Ma							
SSM-1 180–250 μm; $J = 0.002551 \pm 0.000006$; weight = 2.75 mg							
850	6.05	0.03478	0.9168	27.3	37.2	2.6	27.7 ± 1.2
900	7.88	0.01648	0.3164	58.0	61.9	7.0	35.9 ± 0.6
950	8.32	0.00434	0.0710	178.0	86.7	28.7	37.9 ± 0.2
975	7.90	0.00575	0.1524	92.9	82.4	15.0	36.0 ± 0.4
1000	7.75	0.00546	0.2065	58.2	82.9	9.6	35.3 ± 0.4
1050	7.90	0.00306	0.1473	79.6	89.8	14.0	36.0 ± 0.4
1100	8.12	0.00229	0.1244	84.0	92.4	14.8	37.0 ± 0.2
1350	9.33	0.00476	0.2608	49.8	87.1	7.2	42.4 ± 0.4
1650	9.82	0.05341	1.9380	18.1	38.6	1.1	44.7 ± 2.4
Total gas age = 37.0 ± 0.4 Ma							
CSM-1 20–63 μm; $J = 0.004831 \pm 0.000024$; weight = 3.39 mg							
800	3.45	0.00650	0.0033	25.4	62.0	3.8	29.8 ± 0.7
850	3.69	0.00220	0.0011	34.2	75.4	5.8	31.9 ± 0.5
900	3.93	0.00100	0.0005	45.1	85.3	8.1	33.9 ± 0.4
950	4.13	0.00030	0.0001	77.4	93.4	14.5	35.6 ± 0.6
975	4.22	0.00010	0.0001	84.8	97.0	16.2	36.4 ± 1.1
1000	4.28	0.00000	0.0000	76.4	96.4	14.3	36.9 ± 0.6
1050	4.37	0.00000	0.0000	91.8	97.8	17.0	37.7 ± 0.5
1100	4.45	0.00080	0.0004	71.9	98.1	13.2	38.3 ± 0.5
1350	5.45	0.09660	0.0493	43.5	95.0	6.3	46.9 ± 0.6
1650	43.82	0.25570	0.1305	52.6	87.9	0.9	346.4 ± 6.8
Total gas age = 39.5 ± 0.6 Ma							
CSM-1 180–250 μm; $J = 0.004815 \pm 0.000024$; weight = 3.98 mg							
800	3.11	0.01864	0.0070	48.6	36.1	4.0	26.8 ± 1.0
850	3.49	0.00724	0.0045	44.6	62.0	5.6	30.1 ± 0.6
900	3.69	0.00510	0.0028	61.4	71.0	8.4	31.8 ± 0.4
950	4.16	0.00100	0.0015	133.3	93.4	21.2	35.8 ± 0.4
975	4.22	0.00046	0.0017	101.1	96.9	16.4	36.3 ± 0.4
1000	4.25	0.00042	0.0017	67.3	97.2	10.9	36.6 ± 0.4
1050	4.32	0.00036	0.0011	104.0	97.6	16.6	37.1 ± 0.4
1100	4.32	0.00042	0.0017	61.7	97.2	9.8	37.1 ± 0.4
1350	5.95	0.00117	0.0056	53.8	94.5	6.0	50.9 ± 0.6
1650	30.73	0.01725	0.0164	57.5	85.8	1.1	248.9 ± 3.4
Total gas age = 38.6 ± 0.4 Ma							
CSM-2 20–63 μm; $J = 0.004831 \pm 0.000024$; weight = 3.19 mg							
800	3.36	0.88800	0.4530	25.0	68.6	4.5	29.1 ± 0.7
850	3.63	0.02810	0.0143	30.5	90.0	6.7	31.4 ± 0.5
900	3.84	0.01440	0.0073	37.9	96.3	8.4	33.2 ± 0.5
950	4.02	0.00900	0.0046	56.5	97.9	12.2	34.7 ± 0.5
975	4.19	0.00450	0.0023	61.0	99.0	12.8	36.1 ± 0.5
1000	4.21	0.00260	0.0013	59.4	98.9	12.3	36.3 ± 0.5
1050	4.31	0.00170	0.0009	82.3	98.2	16.6	37.2 ± 0.5
1100	4.38	0.00040	0.0002	89.0	99.3	17.8	37.8 ± 0.5
1350	4.97	0.07850	0.0400	51.2	94.2	8.6	42.8 ± 0.6
1650	106.11	0.50160	0.2559	23.2	70.0	0.1	746.6 ± 28.0
Total gas age = 37.2 ± 0.6							
CSM-2 180–250 μm; $J = 0.004831 \pm 0.000024$; weight = 4.40 mg							
800	2.93	0.00392	0.0235	61.0	71.7	8.4	25.3 ± 0.4
850	3.41	0.00054	0.0025	62.1	95.5	9.7	29.5 ± 0.4
900	3.81	0.00025	0.0020	83.5	98.1	12.1	32.9 ± 0.4

Table 2 (*continued*)

Temp (°C)	$^{40}Ar^*/^{39}Ar$	$^{36}Ar/^{39}Ar$	$^{37}Ar/^{39}Ar$	^{40}Ar (mol ($\times 10^{-14}$))	$\%^{40}Ar^*/\%^{39}Ar$	Rel. age $\pm 2\sigma$ (Ma)	
950	4.21	0.00019	0.0017	146.7	98.7	19.3	36.3 ± 0.4
975	4.27	0.00019	0.0012	122.1	98.7	15.8	36.9 ± 0.4
1000	4.32	0.00018	0.0012	88.4	98.8	11.3	37.3 ± .4
1050	4.34	0.00015	0.0010	97.4	99.0	12.4	37.5 ± 0.4
1100	4.36	0.00019	0.0009	61.4	98.7	7.8	37.6 ± 0.4
1350	5.22	0.00060	0.0193	23.6	96.7	2.5	45.0 ± 0.8
1650	26.49	0.01150	0.0769	37.1	88.7	0.7	217.3 ± 3.2
Total gas age = 36.2 ± 0.4 Ma							
ESM-2 20–63 μm; $J = 0.002553 \pm 0.000006$; weight = 2.50 mg							
800	4.01	0.01035	0.7010	15.8	57.2	3.8	18.4 ± 0.6
850	4.83	0.00719	0.4739	19.7	69.8	4.8	22.1 ± 0.4
900	5.48	0.00498	0.3300	27.7	79.1	6.7	25.1 ± 0.4
950	6.16	0.00284	0.1076	72.5	88.1	17.4	28.1 ± 0.2
975	6.20	0.00271	0.1225	71.9	88.7	17.2	28.4 ± 0.2
1000	6.19	0.00329	0.1493	59.2	86.5	13.9	28.3 ± 0.2
1050	6.47	0.00247	0.1126	87.5	90.0	20.4	29.6 ± 0.2
1100	6.40	0.00277	0.1859	49.6	88.8	11.5	29.2 ± 0.2
1350	5.68	0.00695	0.6963	19.5	74.0	4.3	26.0 ± 0.6
Total gas age = 27.7 ± 0.2							
ESM-2 180–250 μm; $J = 0.002567 \pm 0.000006$; weight = 2.78 mg							
800	2.95	0.00939	0.7368	11.2	52.0	2.8	13.6 ± 0.6
850	3.54	0.00764	0.7059	10.9	61.6	2.7	16.3 ± 0.6
900	4.58	0.00680	0.5988	14.9	70.0	3.3	21.1 ± 0.4
950	6.85	0.00240	0.0610	122.9	90.7	23.3	31.5 ± 0.2
975	6.70	0.00217	0.1122	75.0	91.4	14.6	30.7 ± 0.2
1000	6.40	0.00325	0.1751	43.0	87.1	8.4	29.4 ± 0.2
1050	6.76	0.00187	0.0889	87.4	92.5	17.1	31.0 ± 0.2
1100	6.60	0.00260	0.1761	50.1	89.7	9.8	30.3 ± 0.2
1350	6.80	0.00180	0.1089	77.4	92.8	15.1	31.2 ± 0.2
1650	5.68	0.02629	0.6126	26.9	42.4	2.9	26.1 ± 1.2
Total gas age = 29.6 ± 0.2 Ma							

1997; Jaboyedoff and Cosca, 1999). Dynamic recrystallization, as inferred from natural samples, may commonly accommodate the recovery of grains strained by dislocation glide, as observed in experiments. To our knowledge, no evidence has ever been reported for dynamic recrystallization of micas by subgrain rotation, apparently because of the limited types of mobile dislocations in sheet silicates (Etheridge and Hobbs, 1974; Christofferson and Kronenberg, 1993). Good evidence exists, however, for dynamic recrystallization of micas by grain boundary migration at relatively high metamorphic grades (O'Hara and Gromet, 1983). Mica grains that show little internal strain, straight grain boundaries, and a preferred mica grain size may provide evidence for this deformation mechanism (Gromet, 1991; Scheuber et al., 1995).

We focus on three observations in order to understand the deformation history of mica grains in these samples. First, in each sample, micas are phengitic, show a range of grain sizes, and the smaller and larger grains are compositionally alike. The phengitic composition of mica and the absence of detrital mica in the undeformed Permo–Triassic protolith are good evidence that mica grew during Alpine deformation and metamorphism (Sartori, 1990). Although white mica composition depends strongly on pressure and temperature conditions during crystallization (Guidotti, 1984), the relative simplicity of mineral assemblages in these samples suggests that mica compositions may have been constrained by the paucity of mineral exchange options rather than metamorphic conditions. Nonetheless, the similar composition of differently sized grains is consistent with the hypothesis that they crystallized under the same metamorphic conditions. Further microprobe analyses (not reported here) show that large micas lack compositional zoning, indicating that these micas crystallized relatively quickly with respect to changing metamorphic conditions. These observations suggest that, within each sample, micas of different grain sizes crystallized quickly and simultaneously with respect to Alpine orogenesis.

Second, micas with high aspect ratios parallel foliation and those with lower aspect ratios more commonly lie at an angle to foliation. Markley et al. (1998) argued that this relationship between aspect ratio and orientation suggests that mica neocrystallization followed by rigid rotation during noncoaxial deformation best describes the mechanism by which micaceous foliation developed in all four samples. This argument, however, ignores the weakness of mica. In experiments on micaceous quartzites, Shea and Kronenberg (1993) found that mica, even at lower modal concentrations than in the samples described here, always accommodated more deformation than quartz. The observed

relationship between mica grain size, aspect ratio, and orientation may instead offer evidence of dynamic recrystallization of mica by grain boundary migration. The location of the coarsest grains in layers of high modal mica is consistent with the dynamic recrystallization of mica. The lack of compositional zoning in large grains and the compositional homogeneity of grains of different sizes within samples is also consistent with dynamic recrystallization.

Third, micas in samples from the central Siviez-Mischabel (CSM-1 and CSM-2) have a grainy texture, but micas from the eastern and southern Siviez-Mischabel (ESM-2 and SSM-1) have a clear texture in thin section. We speculate that the CSM micas are crystallographically distressed by higher dislocation or microfracture densities than the ESM and SSM micas. Although all samples, and particularly all mica populations, appear to have accommodated high strains, the ESM and SSM micas may have recovered more completely than the CSM micas. Because higher temperatures encourage recovery by grain boundary migration, our interpretation of mica textures is consistent with our inferences from quartz microstructures that the southern and eastern Siviez-Mischabel experienced higher temperatures during Eocene Alpine deformation than the central Siviez-Mischabel.

2.4. Hypotheses relating sample fabrics and dates

There are two basic observations about the white mica dates presented here: dates vary with region, and the relationship between date and grain size varies with region. Specifically, $^{40}Ar/^{39}Ar$ dates from the central Siviez-Mischabel and the southern Siviez-Mischabel (CSM and SSM) agree with independent estimates of the timing of white mica growth during nappe emplacement (Barnicoat et al., 1995; Markley et al., 1998), but those from the eastern Siviez-Mischabel (ESM) are younger by 5–10 m.y. For the ESM and SSM samples, dates of the 20–63-μm-size fraction are 2–3 m.y. younger than dates from the 180–250-μm-size fraction. But for the CSM samples, dates of both size fractions are identical. This relation between date and grain size is a focus of our modeling, and we believe that the dated mica grains maintained their size during separation from the rock. The brittle strength of mica is anisotropic, and white mica generally delaminates rather than breaking at high angles to the basal plane. Because the radial diameter of mica is the critical dimension for argon volume diffusion, mica strength in this orientation suggests that crushing and sieving does not change its size fraction. We therefore make the untestable assumption that the micas in the separated and dated fractions accurately reflect grain sizes in the rock samples.

Markley et al. (1998) first hypothesized that grain size is the effective diffusion dimension (EDD) of micas in this study. If so, the invariance of date with grain size for the CSM samples suggests that these dates record mica growth during nappe emplacement. This first hypothesis is consistent with peak temperatures inferred from quartz and mica fabrics because the CSM samples appear to have experienced lower temperatures than the others and might therefore have been less susceptible to thermally activated radiogenic argon loss through volume diffusion. This first hypothesis is also consistent with independent constraints on the timing of nappe emplacement.

A second hypothesis is that the EDD of micas in this study varies regionally, such that the EDD of the grainy and apparently distresssed micas from the CSM may be smaller than either separated size fraction. The relationship between date and grain size is consistent with this hypothesis, which does not constrain the tectonic significance of the dates. If the CSM micas record cooling or resetting, the good agreement between these dates and the timing of the growth of mica in the Siviez-Mischabel nappe suggests either that resetting was slight or that cooling was rapid following peak deformation and metamorphism.

Below, we present models of the relation between $^{40}Ar/^{39}Ar$ dates and the thermal evolution of the Siviez-Mischabel Nappe. We use the models to explore the two hypotheses above and to further constrain the thermal histories of the ESM and SSM. For these two regions of the Siviez-Mischabel, the positive relation between date and grain size suggests that the EDD of these micas is the grain size and that these dates record post-growth cooling or resetting during a later thermal disturbance.

3. Thermal modeling

DIFFARG (Wheeler, 1996) is a finite difference model that simulates the evolution of argon concentration and zoning in minerals. DIFFARG assumes that potassium, the radioactive parent of argon, is homogeneously distributed throughout the mineral grain and that minerals are initially free of inherited argon. As potassium decays through time to produce radiogenic argon, a cylindrical geometry best describes argon volume diffusion geometry in mica:

$$\nabla^2 C = \partial^2 C/\partial r^2 + (1/r)\partial C/\partial r \quad (1)$$

where C is argon concentration and r is the grain radius. DIFFARG uses this geometry to solve Fick's second law:

$$\partial C/\partial t = D\nabla^2 C + S \quad (2)$$

for a row of elements parallel to the mica basal plane. S is a source term, and D is a function of temperature described by the Arrhenius equation:

$$D = D_0 e^{-(E/RT)} \quad (3)$$

where D_0 is a pre-exponential factor, E is activation energy, R is a gas constant, and T is temperature (itself a function of time and therefore a boundary condition in models). Based on a recalculation (Hames and Bowring, 1994) of the

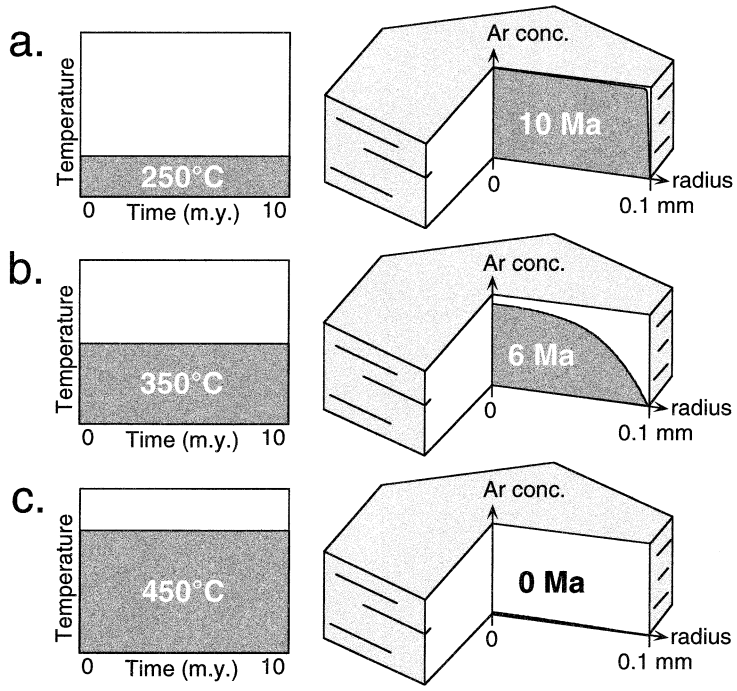

Fig. 7. Results of three simple DIFFARG (Wheeler, 1996) runs for grains 200 μm in radial diameter. Micas grow at time $t = 0$ and remain at 250, 350, or 450 °C for 10 m.y. In each run, DIFFARG monitors the argon concentration at each of the 100 elements and calculates a bulk date by integration of the concentration as a function of the grain radius. (a) After 10 m.y. at 250 °C, the mica retains all of its radiogenic argon and yields a date of 10 Ma. (b) After 10 m.y. at 350 °C, which is the most commonly cited closure temperature (T_c) for white mica, the mica retains a little more than half its radiogenic argon and yields a date of 6 Ma. (c) After 10 m.y. at 450 °C, the mica loses of its radiogenic argon and yields a date of 0 Ma.

original Robbins (1972) results, we use values for white mica of $D_0 = 0.04$ cm^2/s and $E = 52$ kcal/mol in all model runs. A range of estimates for these values exists in the literature (Kirschner et al., 1996; Hames and Cheney, 1997), and our choice does not qualitatively affect the model results. The model runs presented below use 100 equally spaced elements with $C = 0$ at the outermost element in order to mimic a grain boundary network free of argon. This value probably underestimates the concentration of argon in natural grain boundary networks. Unfortunately, very little quantitative work addresses the problem of argon partitioning between K-rich minerals and fluids in grain boundary networks. For discussion and review of published data, see Wheeler (1996).

DIFFARG assumes that argon loss from minerals occurs by volume diffusion activated at high temperatures. This diffusion acts to dampen argon concentration gradients. Fig. 7 shows the results of three simple DIFFARG runs using the parameters discussed above in order to give the reader a feel for the model systematics. In all three models, a white mica grain 200 μm in diameter grows at time $t = 0$ and remains at the same temperature for 10 m.y. DIFFARG successfully mimics the natural temperature range of 250 to 450 °C in which white mica appears to undergo the transition from open to closed system behavior with respect to argon. A mica that grows and remains at 250 °C for 10 m.y. retains all of its radiogenic argon and yields a date of 10 Ma (Fig. 7a); in contrast, a mica that grows and remains at 450 °C for 10 m.y. loses all of its radiogenic argon by volume diffusion and yields a date of 0 Ma (Fig. 7c). Fig. 7b shows a DIFFARG model of argon zoning in a mica that grows and remains for 10 m.y. at 350 °C, the most commonly cited closure temperature (T_c) for white mica. This mica yields a date of 6 Ma because it retained 60% of its radiogenic argon.

Figs. 8–10 show the results of more complex DIFFARG models intended to mimic possible thermal histories of mica in the Siviez-Mischabel Nappe. In all models, instantaneous grain growth occurs at 40 Ma. In the 'linear cooling' models presented in Fig. 8, mica cools from peak metamorphic temperatures at a rate of 10 °C/m.y. in accordance with fission track data (Fig. 2). In the 'pulse' models presented in Fig. 9, mica experiences pulses of elevated temperature ending at 15 Ma. This second set of models explores the possible effects of a transient thermal pulse in the eastern Siviez-Mischabel related to activity along the Simplon Fault Zone. A third set of 'hybrid' models (Fig. 10) explores constant peak temperatures for the first 5 m.y. followed by linear cooling at a rate of 10 °C/m.y. These models consider a lengthier peak metamorphic event than the models in Fig. 8, but they are otherwise similar to the linear cooling models. For all thermal histories, we present results in terms of total gas ages of mica grains both 20 and 200 μm in diameter. These grain sizes approximate the 20–63 μm and 180–250 μm size fractions separated and dated from the Siviez-Mischabel.

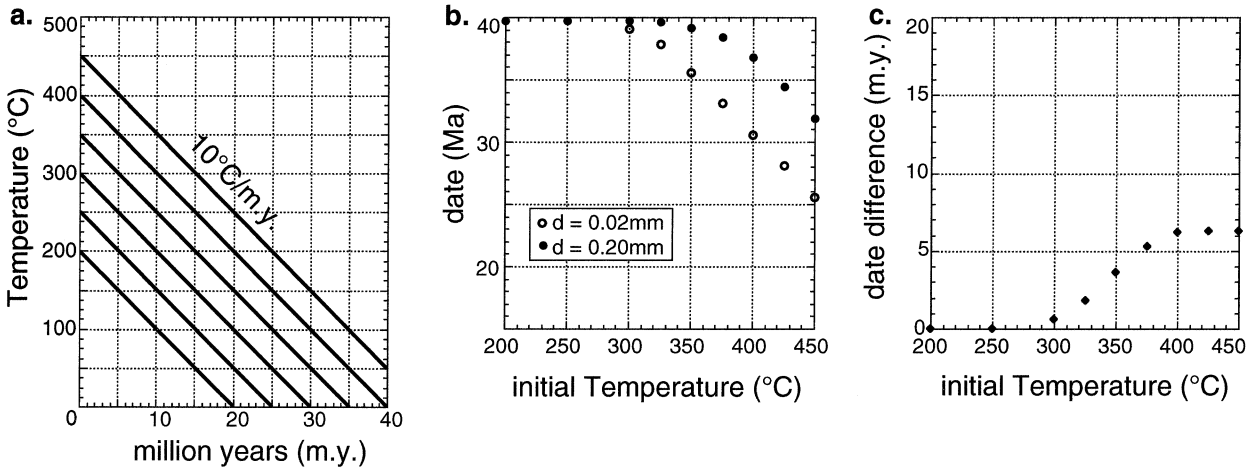

Fig. 8. Results of DIFFARG linear cooling models. See text for discussion.

In the model results, most mica yield dates significantly younger than the timing of mica growth at 40 Ma. In addition, argon loss is generally more significant for smaller grains than for larger grains that share the same thermal history. Differences in dates for two micas of different size that share the same thermal history range from 0 to 20 m.y.

3.1. Linear cooling models

Model results from simple linear cooling histories (Fig. 8) have interesting implications for closure temperatures in metamorphic systems. Fig. 8a shows linear cooling histories that suit Dodson's (1973) criteria for defining T_c *sensu*

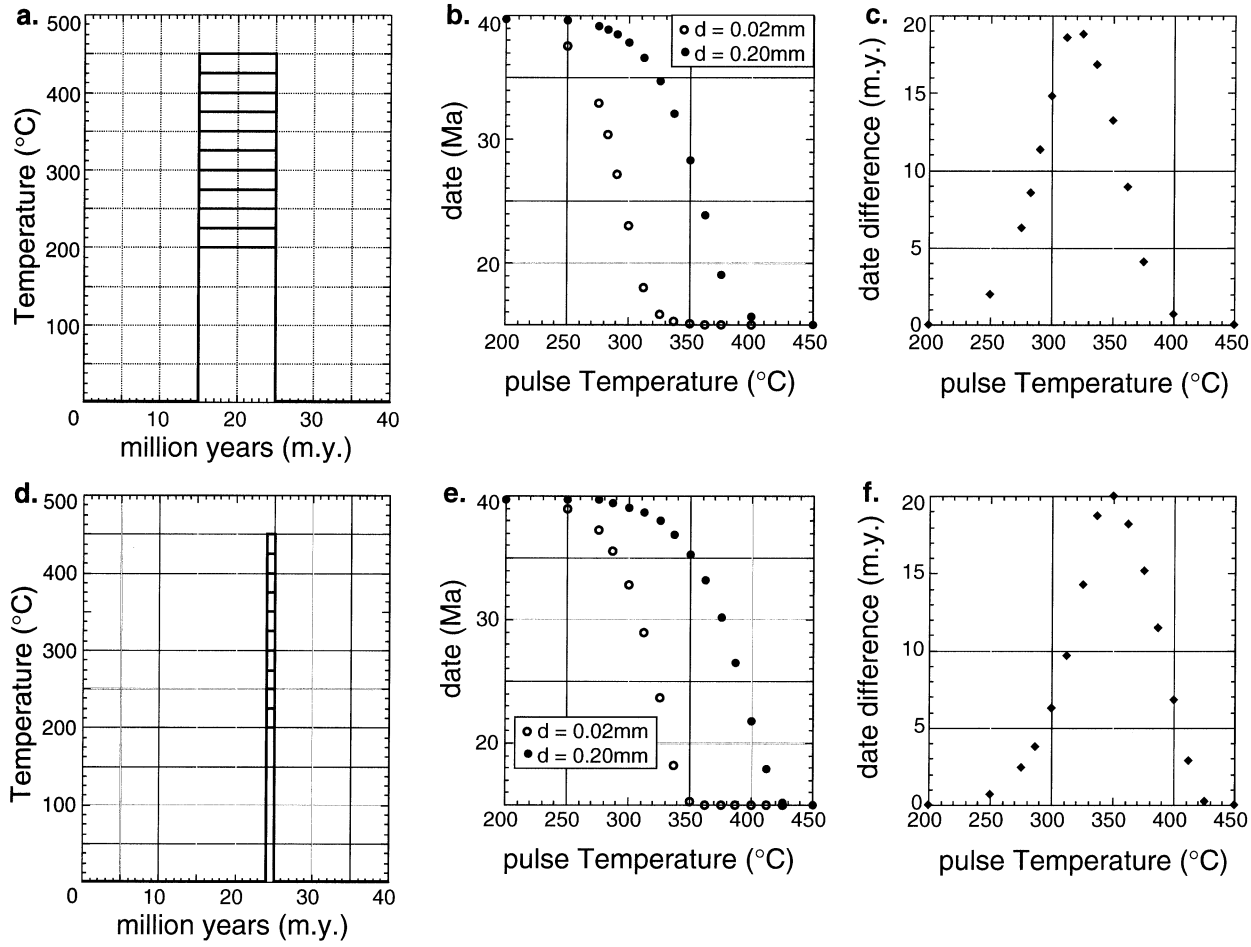

Fig. 9. Results of DIFFARG thermal pulse models. See text for discussion.

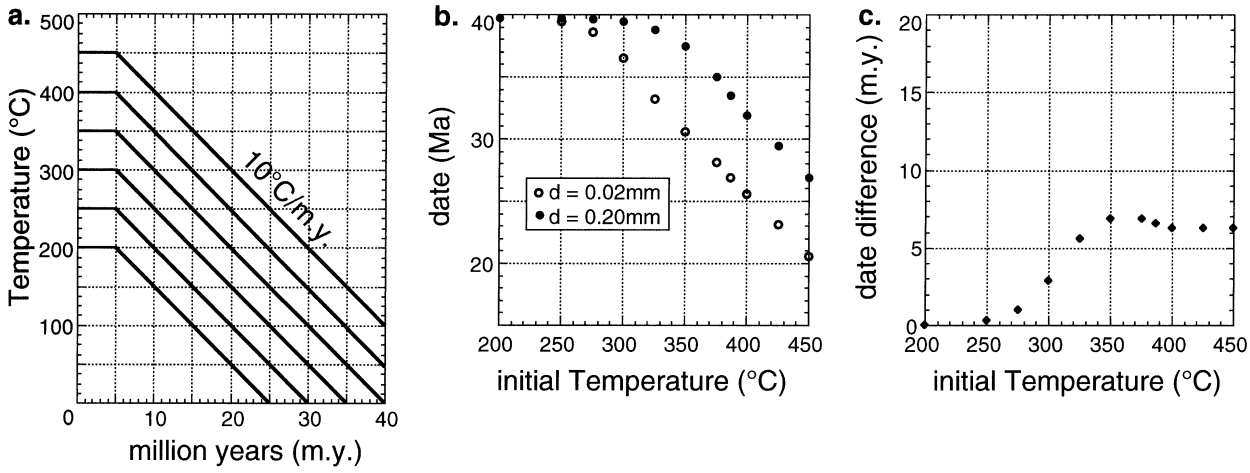

Fig. 10. Results of DIFFARG hybrid models. See text for discussion.

stricto. For example, in the linear cooling history where white mica grow at 450 °C and immediately begin cooling at a rate of 10 °C/m.y., the 200 μm grain yields a cooling age of 32 Ma, at which time its temperature was 370 °C, and the 20 μm grain yields a cooling age of 26 Ma, at which time its temperature was 310 °C (Fig. 8a and b). For the temperature history where mica grow at 425 °C and cool at the same rate, the 200 and 20 μm grains yield different cooling ages, 34 and 28 Ma, respectively, but these dates still correspond to the times at which the temperatures were 370 and 310 °C. Micas that grow and cool from higher initial temperatures therefore exhibit *sensu stricto* closure temperatures, and the T_c of 200 and 20 μm grains with a 10 °C/m.y. cooling rate are 370 and 310 °C, respectively. In this case, the maximum difference in date between two grains that share the same thermal history is 6 m.y. (Fig. 8c). This difference is a function of grain size and cooling rate. Faster cooling rates yield smaller maximum differences in date, and slower cooling rates yield larger maximum differences in date. In cases where there is no difference in date between two grain sizes that share the same thermal history, dates are 40 Ma and record mica growth.

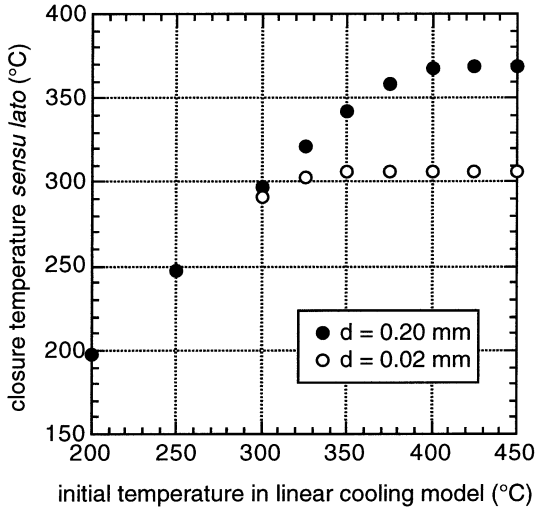

Fig. 11. The relation between initial temperature in the linear cooling model (Fig. 8) and closure temperature *sensu lato*: "temperature at the time corresponding to the age of the mineral" (Dodson, 1973). At low initial temperatures, a one-on-one relation exists between initial temperature and closure temperature. At high initial temperatures, closure temperature is independent of initial temperature.

Fig. 11 looks in more detail at this phenomenon by examining the relation between initial temperature in the linear cooling model and closure temperature *sensu lato*: "temperature at the time corresponding to the age of the mineral" (Dodson, 1973). At low initial temperatures (300 °C and below), a one-on-one relation exists between initial temperature and closure temperature. In other words, mica yields growth ages because temperatures are too low to encourage argon loss. At high initial temperatures, as discussed above, closure temperature is independent of initial temperature, and micas yield cooling ages that record the time at which they passed through T_c *sensu stricto*. Fig. 11 shows that, although its T_c is 370 °C, the 200 μm grain exhibits a transition between growth ages and cooling ages for initial temperatures between 350 and 400 °C. The 20 μm grain, whose T_c is 310 °C, shows the same relation, but the transition from growth ages to cooling ages occurs over a lower temperature range, between 250 and 350 °C. Thus some grains that grow at temperatures below T_c yield dates that are not growth ages because they experience partial argon loss, and some grains that grow above T_c yield dates that are not cooling ages.

3.2. Pulse models

The results of pulse models (Fig. 9) also caution against simplifying argon behavior in mica in terms of open system behavior above T_c and closed system behavior below T_c. Mica that experience thermal pulses of 10 and 1 m.y. in duration at temperatures well below T_c show significant

argon loss (Fig. 9b and e). This feature of the pulse models probably relates to the high argon concentrations accumulated in the grains during their first 15–25 m.y., during which time the micas remain at 0 °C and do not leak. Pulses of high temperature that follow cause such pronounced argon loss because of the steep initial concentration gradient between the more mature, argon-rich grains and the argon-free grain boundary network. For example, a 200 μm grain experiencing a thermal pulse of 350 °C (20 °C below its T_c as calculated for cooling rates explored above) shows significant argon loss and yields a date of 28 Ma. This date underestimates the growth of the mineral by 12 m.y. A 20 μm grain experiencing the same thermal history loses all of its radiogenic argon, and its date is completely reset to 15 Ma, the time of instantaneous cooling at the end of the thermal pulse. This example highlights another interesting feature of the pulse models: large differences in date for different grain sizes experiencing the same thermal history. This difference in date between the two grain sizes is most pronounced (up to 20 m.y.) around 325 °C for 10 m.y. thermal pulses and around 350 °C for 1 m.y. pulses (Fig. 9c and f). At extremely low pulse temperatures (250 °C and below), mica retains radiogenic argon and both grain sizes yield the same growth age of 40 Ma. This phenomenon is identical to the lower temperature linear cooling histories where, if both grain sizes share the same date for the same thermal history, dates record mica growth. At extremely high pulse temperatures (425 °C and above), however, both grain sizes also share the same date for the same thermal history, but dates are 15 Ma and record complete argon loss during the thermal pulse followed by instantaneous cooling.

3.3. Hybrid models

The hybrid models (Fig. 10) are similar to the linear models except for two results. First, for the same initial temperatures as the linear models, mica in the hybrid models show more significant argon loss and yield younger dates (Fig. 10b). This result is intuitive, because the hybrid models remain 5 m.y. at initial temperatures before cooling at a rate of 10 °C/m.y. Second, the difference in date between the two grain sizes is most pronounced (7 m.y.) for initial temperatures around 350 °C (Fig. 10c). This result is counter-intuitive and more similar to the pulse models. At higher initial temperatures (400 °C and above), however, the hybrid models behave like the linear models and the difference in date between the two grain sizes is 6 m.y., a function of cooling rate. One other feature of these models that is similar to the linear cooling models is that dates are 40 Ma and record mica growth in cases where both grain sizes share the same date for the same thermal history.

4. Discussion

The purpose of comparing model results with $^{40}Ar/^{39}Ar$ dates is threefold: (1) to investigate the two hypotheses regarding the effective diffusion dimension (EDD) of mica in the central Siviez-Mischabel (samples CSM-1 and CSM-2); (2) to further constrain the tectonic significance of dates acquired from the eastern and southern Siviez-Mischabel nappe (samples ESM-2 and SSM-1); and (3) to explore whether dates from the three regions are best described as recording mica growth, later cooling, or thermal resetting. Dates may be directly compared with model results by assuming that argon loss from mica occurs by thermally activated volume diffusion (i.e. the EDD is the grain size itself) or that the effect of multipath diffusion is to lower the EDD in a relatively simple manner (i.e. a larger grain behaves as a smaller grain with respect to argon diffusion). In the following discussion, we cite precise temperatures; however, uncertainty in the diffusion parameters of argon in white mica (Hames and Bowring, 1994; Kirschner et al., 1996; Hames and Cheney, 1997) means that these temperatures are qualitatively rather than quantitatively appropriate to our arguments. In addition, we assume that mica growth in all samples occurred during nappe emplacement during the latest Eocene (around 40–37 Ma).

If the grain size is the EDD for mica in the central Siviez-Mischabel samples, then models show that dates probably record mica growth during nappe emplacement. The simplest models, the linear cooling models in Fig. 8, agree well with dates from the CSM. If mica grew at peak metamorphic temperatures of 300 °C and cooled linearly at 10 °C/m.y. during exhumation of the Siviez-Mischabel (Fig. 8), both grain sizes yield statistically indistinguishable dates that record mica growth. Therefore, mica dates of 40–36 Ma for both analyzed grain sizes from the central Siviez-Mischabel may reflect mica growth during peak deformation and metamorphism in the Siviez-Mischabel at approximately 300 °C. This estimate of the timing of mica growth associated with nappe emplacement agrees well with the arguments of Markley et al. (1998).

If the EDD is significantly smaller than grain size for mica in the CSM samples, perhaps indicated by the grainy texture of these micas, then these dates may slightly postdate mica growth. Again, the simple linear cooling models (Fig. 8) agree well with dates from the CSM. For example, if the EDD of all grains is 20 μm and mica grew at peak metamorphic temperatures of 325 °C, then the dates of these micas underestimate the timing of mica growth by a few million years (Fig. 8). Regardless of the EDD for CSM micas, linear cooling models explain date relations in the central Siviez-Mischabel. Dates from CSM micas are consistent with a simple cooling history and inferences from quartz microstructures that the central Siviez-Mischabel experienced relatively low temperatures.

For the sample from the southern Siviez-Mischabel, models show that dates probably record some diffusive argon loss due to slightly higher temperatures. The difference in date between the two size fractions of mica strongly suggests that the EDD is the grain size itself. The sample from the southern Siviez-Mischabel yields a 3 m.y.

difference between the two grain sizes and a date of the larger size fraction of 37 Ma. These observations may correspond to mica cooling ages recording a peak metamorphic temperature of 350 °C followed by linear cooling (Fig. 8). Dates from SSM micas are therefore consistent with a simple linear cooling history and inferences from quartz microstructures that the southern Siviez-Mischabel experienced higher peak temperatures than the central Siviez-Mischabel.

None of the models yields relations that exactly match dates from the eastern Siviez-Mischabel, where there is a 2 m.y. difference between dates of the two grain sizes and the larger size fraction yields a relatively young date of 30 Ma. For example, in the linear cooling models (Fig. 8), a peak metamorphic temperature of 450 °C followed by linear cooling produces a date of about 30 Ma for the larger size fraction, but the difference in date predicted for the two grain sizes is 6 m.y. Nor do dates agree with results of thermal pulse models (Fig. 9) designed to mimic possible transient high temperatures in the eastern Siviez-Mischabel following its juxtaposition against the lower Pennine nappes along the Simplon normal fault about 15 Ma (Graseman and Mancktelow, 1993; Steck and Hunziker, 1994). Except in the case that mica dates are unaffected by the pulse and record growth at 40 Ma and the case that mica dates are completely reset to 15 Ma, these pulse models produce extremely large differences in date between the two grain sizes. Like the linear cooling models, the hybrid models (Fig. 10) also yield date differences between grain sizes that are too large to agree with the data and explain a relatively young date for the largest grain size. Therefore, the thermal history of the eastern Siviez-Mischabel does not correspond simply to any of the models presented here and may differ significantly from that of the other regions. Thus the thermal effects of the Simplon Fault Zone are probably not well represented by these models.

The above interpretations are not unique, and other explanations for the observed dates exist. We briefly review three possibilities here. First, the samples from the eastern Siviez-Mischabel may be strongly influenced by the 30 Ma magmatism in the nearby lower Pennine nappes (Steck and Hunziker, 1994; Schärer et al., 1996). We did not attempt to model this scenario. Second, the EDD of mica in these samples may be a more complex problem than we envision. For example, the EDD of the larger micas from the ESM and SSM samples may be smaller than the grain size but larger than that of the smaller micas. Or, the EDD of these white micas may be more complicated again and not well characterized by a simple linear quantity. The question of how to characterize the EDD of white micas remains unresolved in the literature. Third, the tectonic history of the Siviez-Mischabel nappe that we use here (Fig. 2) may be incomplete. As we discussed above, this thermal history is ill-constrained for the late Eocene and early Miocene. The cooling rate of the Siviez-Mischabel nappe following its emplacement may have been extremely rapid for a few million years, and a faster cooling rate may explain the observed relations between grain size and date.

5. Conclusions

Some $^{40}Ar/^{39}Ar$ dates obtained from Alpine white mica from the cover units of the Siviez-Mischabel Nappe record mica growth during deformation and metamorphism associated with nappe emplacement at 40–36 Ma during Alpine orogenesis. Variations in the $^{40}Ar/^{39}Ar$ dates, however, relate to regional variations in the thermal history of the nappe. A comparison of dates with DIFFARG (Wheeler, 1996) model results supports inferences from rock fabrics that the southern Siviez-Mischabel nappe experienced higher peak temperatures than the central Siviez-Mischabel, even though dates obtained on mica in both regions agree with the timing of mica growth. Dates obtained from the eastern Siviez-Mischabel nappe do not compare well with simple models, however, and the thermal evolution of this region of the nappe is not well understood.

Acknowledgements

Thanks to John Wheeler for use of DIFFARG, and to Bill Hames, Simon Kelley, and Dirk Slawinski for help modifying and running DIFFARG. Thoughtful, critical reviews by Peter Gromet, Kip Hodges, and Mike Williams significantly improved this manuscript. MJM thanks the American Association of University Women for support during the revision of this manuscript. Dating in this study was supported by the Swiss National Science Foundation (2000-056849). Field research was supported by the U.S. National Science Foundation (EAR 9206118).

References

Argand, E., 1916. Sur l'arc des Alpes Occidentales. Eclogae Geologicae Helvetiae 14, 145–204.

Barnicoat, A.C., Rex, D.C., Guise, P.G., Cliff, R.A., 1995. The timing and nature of greenschist facies deformation and metamorphism in the upper Pennine Alps. Tectonics 14, 279–293.

Behrmann, J.H., 1984. A study of white mica microstructure and microchemistry in a low grade mylonite. Journal of Structural Geology 6, 283–292.

Bell, I.A., Wilson, C.J.L., 1981. Deformation of biotite and muscovite; TEM microstructure and deformation model. Tectonophysics 78, 201–228.

Bell, T.H., 1978. Syntectonic nucleation of new grains in deformed mica. Tectonophysics 51, T31–T37.

Christofferson, R., Kronenberg, A.K., 1993. Dislocation interactions in experimentally deformed biotite. Journal of Structural Geology 15, 1077–1095.

Cosca, M.A., Hunziker, J.C., Huon, S., Masson, H., 1992. Radiometric age constraints on mineral growth, metamorphism, and tectonism in the Gumfluh Klippe, Briançonnais domain of the Préalpes, Switzerland. Contributions to Mineralogy and Petrology 112, 439–449.

de Jong, K., Wijbrans, J.R., Féraud, G., 1992. Repeated thermal resetting of phengites in the Mulhacen Complex (Betic Zone, southeatern Spain)

shown by $^{40}Ar/^{39}Ar$ step heating and single grain laser probe dating. Earth and Planetary Science Letters 110, 173–191.

Dodson, M.H., 1973. Closure temperature in cooling geochronological and petrological systems. Contributions to Mineralogy and Petrology 40, 259–274.

Dong, H., Hall, C.M., Halliday, A.N., Peacor, D.R., 1997. Laser $^{40}Ar/^{39}Ar$ dating of microgram-size illite samples and implications for thin section dating. Geochimica et Cosmochimica Acta 61, 3803–3808.

Dunlap, W.J., 1997. Neocrystallization or cooling? $^{40}Ar/^{39}Ar$ ages of white micas from low grade mylonites. Chemical Geology 143, 181–203.

Dunlap, W.J., Teyssier, C., McDougall, I., Baldwin, S., 1991. Ages of deformation from K/Ar and $^{40}Ar/^{39}Ar$ dating of white micas. Geology 19, 1213–1216.

Escher, A., 1988. Structure de la nappe du Grand Saint-Bernard entre le val de Bagnes et les Mischabel (Rapport géologique No. 7). Service Hydrologique et Géologique National.

Etheridge, M.A., Hobbs, B.E., 1974. Chemical and deformation controls on recrystallization of mica. Contributions to Mineralogy and Petrology 43, 111–124.

Foland, K.A., Hubacher, F.A., Arehart, G.B., 1992. $^{40}Ar/^{39}Ar$ dating of very fine-grained samples; an encapsulated-vial procedure to overcome the problem of ^{39}Ar recoil loss. Chemical Geology 102, 269–276.

Frank, E., Stettler, A., 1979. K–Ar and Ar–Ar systematics of white K-mica from an Alpine metamorphic profile in the Swiss Alps. Schweizerische Mineralogische und Petrographische Mitteilungen 59, 375–394.

Gilletti, B.J., 1974. Studies in Diffusion I: Argon in phlogopite mica. - In Geochemical Transport and Kinetics (A.W. Hoffman, Ed.), Carnegie Institute, Washington, D.C.

Goodwin, L.B., Renne, P.R., 1991. Effects of progressive mylonitization on Ar retention in biotites from the Santa Rosa mylonite zone, California, and thermochronologic implications. Contributions to Mineralogy and Petrology 108, 283–297.

Graseman, B., Mancktelow, N.S., 1993. Two-dimensional thermal modelling of normal faulting: the Simplon Fault Zone, Central Alps, Switzerland. Tectonophysics 225, 155–165.

Gromet, P.L., 1991. Direct dating of deformational fabrics. In: L. Heaman and J.N. Ludden, Eds. Applications of Radiogenic Isotope Systems to Problems in Geology; Short Course Handbook. Royal Ontario Museum, Toronto, pp. 167–189.

Guidotti, C.V., 1984. Micas in metamorphic rocks. In: S.W. Bailey, Ed. Micas. Mineralogical Society of America 13, pp. 357–467.

Hames, W.E., Bowring, S.A., 1994. An empirical evaluation of the argon diffusion geometry in muscovite. Earth and Planetary Science Letters 124, 161–167.

Hames, W.E., Cheney, J.T., 1997. On the loss of $^{40}Ar^*$ from muscovite during polymetamorphism. Geochimica et Cosmochimica Acta 61, 3863–3872.

Hammerschmidt, K., Stöckhert, B., 1987. A K–Ar and $^{40}Ar/^{39}Ar$ study on white micas from the Brixen Quartzphyllite, Southern Alps: evidence for argon loss at low temperatures. Contributions to Mineralogy and Petrology 95, 393–406.

Hess, J.C., Lippolt, H.J., Gurbanov, A.G., Michalski, I., 1993. The cooling history of the late Pliocene Eldzhurtinskiy granite (Caucasus, Russia) and the thermochronological potential of grain-size/age relationships. Earth and Planetary Science Letters 117, 393–406.

Hodges, K.V., Hames, W.E., Bowring, S.A., 1994. $^{40}Ar/^{39}Ar$ age gradients in micas from a high-temperature–low-pressure metamorphic terrain: evidence for very slow cooling and implications for the interpretation of age spectra. Geology 22, 55–58.

Hunziker, J.C., 1986. The evolution of illite to muscovite: an example of the behaviour of isotopes in low-grade metamorphic terrains. Chemical Geology 57, 31–40.

Itaya, T., Takasugi, H., 1988. Muscovite K–Ar ages of the Sanbagawa schists, Japan and argon depletion during cooling and deformation. Contributions to Mineralogy and Petrology 100, 281–290.

Jaboyedoff, M., Cosca, M.A., 1999. Dating incipient metamorphism using $^{40}Ar/^{39}Ar$ geochronology and XRD modeling: a case study from the Swiss Alps. Contributions to Mineralogy and Petrology 135, 93–113.

Kelley, S., 1988. The relationship between K–Ar mineral ages, mica grain-sizes and movement on the Moine thrust zone, NW Highlands, Scotland. Journal of the Geological Society, London 145, 1–10.

Kerrich, R., Beckinsdale, R.D., Durham, J.J., 1977. The transition between deformation regimes dominated by intercrystalline diffusion and intracrystalline creep evaluated by oxygen isotope thermometry. Tectonophysics 38, 241–257.

Kirschner, D.L., Cosca, M.A., Masson, H., Hunziker, J.C., 1996. Staircase $^{40}Ar/^{39}Ar$ spectra of fine-grained white mica: timing and duration of deformation and empirical constraints on argon diffusion. Geology 24, 747–750.

Knipe, R.J., 1989. Deformation mechanisms—recognition from natural tectonites. Journal of Structural Geology 11, 127–146.

Kramar, N., Cosca, M.A., Hunziker, J.C., 2001. Heterogeneous $^{40}Ar^*$ distributions in naturally deformed muscovite: in situ UV-laser ablation evidence for microstructurally controlled intragrain diffusion. Earth and Planetary Science Letters 192, 377–388.

Lee, J.K.W., 1995. Multipath diffusion in geochronology. Contributions to Mineralogy and Petrology 120, 60–82.

Lo, C.H., Onstott, T.C., 1995. Rejuvenation of K–Ar systems for minerals in the Taiwan Mountain Belt. Earth and Planetary Science Letters 131, 71–98.

Lovera, O.M., Richter, F.M., Harrison, T.M., 1989. The $^{40}Ar/^{39}Ar$ thermochronometry for slowly cooled samples having a distribution of diffusion domain sizes. Journal of Geophysical Research 94, 17917–17935.

Markley, M.J., Teyssier, C., Cosca, M., Caby, R., Hunziker, J.C., Sartori, M., 1998. Alpine deformation and $^{40}Ar/^{39}Ar$ geochronology of synkinematic white mica in the Siviez-Mischabel Nappe, western Pennine Alps, Switzerland. Tectonics 17, 407–425.

McClay, K.R., 1977. Pressure solution and cobble creep in rocks. Journal of the Geological Society of London 134, 57–70.

Mulch, A., Cosca, M.A., Handy, M.R., 2001. In-situ UV-laser $^{40}Ar/^{39}Ar$ geochronology of a micaceous mylonite; an example of defect-enhanced argon loss. Contributions to Mineralogy and Petrology. Online DOI 10.1007/s00410–001–0325–6.

O'Hara, K.D., Gromet, L.P., 1983. Textural and Rb–Sr isoptopic evidence for late Paleozoic mylonitization within the Honey Hill fault zone, southeastern Connecticutt. American Journal of Science 283, 762–779.

Phillips, D., Onstott, T.C., 1988. Argon isotopic zoning in mantle phlogopite. Geology 16, 542–546.

Reddy, S.M., Potts, G.J., Kelley, S.P., Arnaud, N.O., 1999. The effects of deformation-induced microstructures on intragrain $^{40}Ar/^{39}Ar$ ages in potassium feldspar. Geology 27, 363–366.

Reuter, A., Dallmeyer, R.D., 1987. Significance of $^{40}Ar/^{39}Ar$ age spectra of whole-rock and constituent grain-size fractions from anchizonal slates. Chemical Geology (Isotope Geoscience Section) 66, 73–88.

Robbins, G.A., 1972. Radiogenic argon diffusion in muscovite under hydrothermal conditions. M.Sc. Thesis, Brown University.

Sartori, M., 1990. L'unité du Barrhorn (Mémoires de Géologie No. 6). Université de Lausanne.

Scaillet, S., Féraud, G., Lagabrielle, Y., Ballevre, M., Ruffet, G., 1990. $^{40}Ar/^{39}Ar$ laser-probe dating by step-heating and spot fusion of phengites from the Dora Maira nappe of the western Alps, Italy. Geology 18, 741–744.

Schärer, U., Cosca, M., Steck, A., Hunziker, J., 1996. Termination of major ductile strike-slip shear and differential cooling along the Insubric Line (central Alps): U–Pb, Rb–Sr, and $^{40}Ar/^{39}Ar$ ages of cross-cutting pegmatities. Earth and Planetary Science Letters 142, 331–351.

Scheuber, E., Hammerschmidt, K., Friedrichsen, H., 1995. $^{40}Ar/^{39}Ar$ and Rb–Sr analyses from ductile shear zones from the Atacama Fault Zone, northern Chile: the age of deformation. Tectonophysics 250, 61–87.

Shea, W.T., Kronenberg, A.K., 1993. Strength and anisotropy of foliated

rocks with varied mica contents. Journal of Structural Geology 15, 1097–1121.

Soom, M.A., 1990. Abkühlungs- and Hebungsgeschichte der Externmassive und der penninischen Decken beidseits der Simplon-Rhone-Linie seit dem Oligozän: Spaltspurdatierungen an Apatit/Zircon und K–Ar-Datierungen an Biotit/Muskowit (Westliche Zentralalpen). Ph.D., University of Bern, Switzerland.

Steck, A., Hunziker, J., 1994. The Tertiary structural and thermal evolution of the Central Alps—compressional and extensional structures in an orogenic belt. Tectonophysics 238, 229–254.

Vernon, R.H., 1977. Microfabric of mica aggregates in partly recrystallized biotite. Contributions to Mineralogy and Petrology 61, 175–185.

West, D.P., Lux, D.R., 1993. Dating mylonitic deformation by the $^{40}Ar/^{39}Ar$ method; an example from the Norumbega fault zone, Maine. Earth and Planetary Science Letters 120, 221–237.

Wheeler, J., 1996. DIFFARG: a program for simulating argon diffusion profiles in minerals. Computers and Geosciences 22, 919–929.

Wilson, C.J.L., 1973. The prograde microfabric in a deformed quartzite sequence, Mount Isa, Australia. Tectonophysics 19, 39–81.

Wilson, C.J.L., Bell, I.A., 1979. Deformation of biotite and muscovite; optical microstructure. Tectonophysics 58, 179–200.

Wright, N., Layer, P.A., York, D., 1991. New insights into thermal history from a single grain $^{40}Ar/^{39}Ar$ analysis of biotite. Earth and Planetary Science Letters 104, 70–79.

Zingg, A., Hunziker, J.C., 1990. The age of movements along the Insubric Line west of Locarno (northern Italy and southern Switzerland). Eclogae Geologicae Helvetiae 83, 629–644.